2018/3

építőanyag

Journal of Silicate Based and Composite Materials

2018/3

Titanium-based composite synthesis in the combustion regime

A. G. KNYAZEVA ▪ Institute of Strength Physical and Material Science SB RAS
▪ anna-knyazeva@mail.ru
G. A. PRIBYTKOV ▪ Institute of Strength Physical and Material Science SB RAS ▪ gapribyt@mail.ru
Yu. A. CHUMAKOV ▪ Institute of Strength Physical and Material Science SB RAS ▪ chya@ispms.tsc.ru

A. G. KNYAZEVA
Professor, principal researcher of Institute of strength physics and material science SB RAS, professor of Tomsk polytechnic university; scientific interest: macrokinetics, irreversible thermodynamics, mathematical modeling of thermal, mechanical and chemical processes accompanying new material synthesis

G. A. PRIBYTKOV
Principal researcher of Institute of strength physics and material science SB RAS, scientific interest: material science, sintering, combustion

Yu. A. CHUMAKOV
Researcher of Institute of strength physics and material science SB RAS; scientific interest: numerical methods; mathematical modeling of thermal-physical processes

Abstract

The model of composite synthesis on the base of titanium with inclusions of carbides, borides and silicides is analyzed numerically. It was assumed that synthesis is carried out from the mixtures Ti-C, Ti-B and Ti-Si containing the excess of titanium in comparison with stoichiometric relation of components necessary for the formation of TiC, TiB and Ti5Si3. The model is based on the classical ideas of the combustion models with summary reaction. However, it takes into account nonstoichiometric composition of green mixture, dependence of properties on the composition changing during the synthesis and the reaction initiation stage in the igniter. Temperature distribution, conversion level, maximal combustion temperature, reaction zone thickness, and the rate of reaction propagation are determined numerically. The results of the product temperature calculation qualitatively agree with experimental data.
Keywords: composite synthesis, nonstoichiometric mixture, gasless combustion, reaction retardation by reaction product, combustion transition through interface

1. Introduction

Combustion synthesis is an intensively developed scientific field [1,2]. Combustion application to modern technologies connects with the possibility to use the energy of chemical reactions and to obtain the final product with slow energy losses. This method attracts attention by numerous researchers. For example, the combustion synthesis of composite with TiC-inclusions of various phase composition was carried out in [3]. Composite from Ni, Ti and B_4C powder blends was synthesized in [4]. Method SHS was used in [5] to obtain composites from Ni_3Al with inclusions TiC, WC, TaC, etc. Authors [6] studied the physical and chemical phenomena in the reaction of TiO_2, C, Al and the TiC/Alumina composite synthesis. Self sustaining high temperature synthesis (SHS) together with following disintegration is on of possible variant to obtain the powder systems with required structure for application for surface modification and object creation in additive technologies [7]. However irreversible conditions of the synthesis lead to the problems of theoretical and experimental character. For example, when the synthesis is carried out in the regime of layered combustion from the mixtures containing inert component (the component does not participate in the reaction), there is limiting concentration of inert above that reaction front stops. In the double systems Ti-C, Ti-Si, Ti-B, excess titanium powder should play a role of inert addition and should form titanium binder in the product. Dependencies of the maximal product temperature and combustion rate on the elemental composition of the green mixture were investigated in numerous papers; however detailed phase composition of the reaction product does not correspond to theoretical predictions. Temperature and combustion rate decrease monotonically when titanium content increase. Second feature inherent to all three systems consist in the liquid phase formation in the reaction front that play ambiguous

role in the combustion mechanism. Reversible state diagram of Ti-C differs on two other systems because there is a wide area of homogeneity for titanium carbide shifted to titanium. This leads to the formation of nonstoichiometric titanium during the synthesis from powder mixtures with titanium excess instead the predicted composition Ti-TiC: instead 60 volume % of titanium binder real composition gives 26 V% [8] of titanium. Several intermediate compounds present at the reversible state diagram for the systems Ti-Si, Ti-B (three borides and five silicides); however not all phases are observed experimentally after the synthesis.

To study the dynamics of reaction front formation, in this paper, the process of composites synthesis in the systems Ti-C, Ti-Si, Ti-B with Ti excess is investigated numerically in term of classical concept with summary reaction scheme taking into account reaction retardation with product accumulation in the special kinetical function.

2. Problem formulation

To calculate theoretically the combustion rate and product temperature in studied systems we use the model suggested in [9] adding it by the stage the reaction initiation in the igniter and properties dependence on the composition. Generalized model for three systems contains the thermal conductivity equations for igniter (stochiometric mixture 5Ti+3Si) and for the mixture where composites form. Specimen is two-layer cylinder with radius R. First layer has the thickness l, second layer thickness is L (*Fig. 1*).

The second mixture contains the Ti-excess with mass concentration η_e. In a first approximation, we assume that summary reactions correspond to simple reaction schemes

Ti+C *titanium carbide*,
or *Ti+2B* → *titanium boride*,
or *5Ti+3Si* → *titanium silicide*

or summary scheme "Reagent-Product". Reaction initiation in the igniter is carried out by spark. Hence, for reaction depth description only two kinetic equations are necessary – for first and for second layers.

Fig.1. *Illustration to the problem formulation: 1- igniter; 2. pressed-powder compact (reagent)*
1. ábra *Illusztráció a probléma értelmezéséhez: 1- a gyújtófej; 2. a préselt (reagens) test*

As a result, we come to the mathematical model:

$$c_1\rho_1\frac{\partial T_1}{\partial t} = \frac{\partial}{\partial x}\left(\lambda_1\frac{\partial T_1}{\partial x}\right) + Q_1\phi_1(\eta_1,T_1) - \frac{2\alpha}{R}(T_1-T_0) - \frac{2\varepsilon\sigma_0}{R}\left(T_1^4-T_0^4\right), \qquad x \le l;$$

$$\frac{d\eta_1}{dt} = \phi_1(\eta_1,T_1) = z_{01}(1-\eta_1)exp\left(-\frac{E_{a1}}{R_gT_1}\right)exp(-m_1\eta_1);$$

$$c_2\rho_2\frac{\partial T_2}{\partial t} = \frac{\partial}{\partial x}\left(\lambda_2\frac{\partial T_2}{\partial x}\right) + Q_2(1-\eta_e)\phi_2(\eta_2,T_2) - \frac{2\alpha}{R}(T_2-T_0) - \frac{2\varepsilon\sigma_0}{R}\left(T_2^4-T_0^4\right), \quad l<x<L;$$

$$\frac{d\eta_2}{dt} = \phi_2(\eta_2,T_2) = z_{02}(1-\eta_2)exp\left(-\frac{E_{a2}}{R_gT_2}\right)exp(-m_2\eta_2) \;;$$

$$x=0: \lambda_1\frac{\partial T_1}{\partial x} = q_0\delta(t);$$

$$x=l: \begin{cases}\lambda_1\dfrac{\partial T_1}{\partial x} = \lambda_2\dfrac{\partial T_2}{\partial x}, \\ T_1 = T_2;\end{cases}$$

$$x=L: -\lambda_2\frac{\partial T_2}{\partial x} = 0;$$

$$t=0: \quad T_1=T_2=T_0, \eta_1=\eta_2=0,$$

where index «1» relates to igniter, index «2» relates to the mixture under study, T – is the temperature, η_k, $k=1,2$, – is the product concentration or conversion level; t – is the time; x – is the spatial coordinate; λ_k, c_k, ρ_k – are the effective thermal conductivity, - unwanted coefficients, heat capacities and densities depending on the current composition; Q_k – are chemical heats of summary reactions; α – is effective heat exchange coefficient in Newton law; σ_0 – is Stephen-Boltzmann constant; ε_0 – is blackness level; $\delta_{(t)}$ – is delta function; E_{ak} – are activation energies; z_{0k} – pre-exponential factors; m_k are the retardation coefficient in formal kinetical laws.

Titanium melting is taken into account through the heat capacity change. Then we can write

$$(c\rho)_{Ti} = \begin{cases}(c\rho)_s, & T<T_{ph,} \\ (c\rho)_L, & T \ge T_{ph,}\end{cases} + Q_{ph}\rho_s\delta\left(T-T_{ph}\right),$$
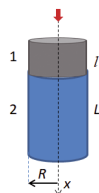
where indexes s and L correspond to the parameters of solid and liquid phases; Q_{ph}- is melting heat; T_{ph} - is melting temperature. Because the powder mixture structure changes during the synthesis and it is not known a priori, we restrict the effective properties calculation by mixture rule, for example, for first layer

$$c_1\rho_1 = [c_{Ti}\rho_{Ti}\eta_{Ti} + c_{Si}\rho_{Si}(1-\eta_{Ti})](1-\eta_1) + c_{Ti5Si3}\rho_{Ti5Si3}\eta_1.$$

The problem was solved numerically. Temperature and concentration fields were found for different time moments that

had allow to find the product temperature and combustion rate for different parameters of the model. The data presented in [10] where used for the calculation (*Table 1*). Formal-kinetical parameters that used for calculations are presented in Table 2 [10-13]. It was assumed: l=1 cm, L=5 cm, R=2.5 cm, a=10^3 W/(m²K), s=5.67×10^{-8} W/(K⁴m²). Other parameters are varied.

Substance	r_s/r_L, kg/m³	λ, W/(m²K)	c_s/c_L, J/(kg×K)	$T_{melting}$, K
Ti	4540/4120	22	498/687	1941
C(graphite)	2250	1.6	712	4620
Si	2330/2520	150	690/979	1687
B	2340	27.4	1280	2075
TiC	4900	21.9	696	3533
Ti₅Si₃	4320	26.8	140	2403
TiB₂	4500	24	656	3503

Table 1. *Thermal-physical properties*
1. táblázat *Hőfizikai tulajdonságok*

Reaction	ΔH$_{react}$, kJ/mol (MJ/kg)	E_a kJ/mol	k_0,1/s	Molar mass, g/mol
Ti+C → TiC	209 (3.5)	117	10^8	60 (TiC)
Ti+2B → TiB₂	295.4(4.25)	123.3	10^8	69.5
5Ti+3Si → Ti₅Si₃	579.3(1.8)	204.2	10^{12}	324(Ti₅Si₃)

Table 2. *Kinetical parameters for the reactions*
2. táblázat *Reakció-kinetikai paraméterek*

3. Result analysis

Reaction front coordinate X_f, reaction front rate (combustion rate) V_f and thickness of the reaction zone X_{ch} were determined similarly to [14]. The retardation parameters were found based on experimental data. It was ascertained for all three systems m_2=10. The comparison of numerical results with experimental data (the experimental method was described, for example, in [8,14]) is presented in *Fig. 2*. For the systems Ti-Si, Ti-B the agreement is very well. For the system Ti-C, there is the deviation of theory from experiment that connects probably with reductive character of the model, where the existence of wide area of homogeneity is not taken into account. Second cause for the deviation connects obviously with the measure of the combustion temperature for the synthesis conditions in air. Titanium oxidation can effect on summary heat release that is confirmed with the data [9], where the presence of titanium dioxide to 8% was detected. With titanium excess η_e increase the combustion temperature decreases.

Calculation for the reaction mixture Ti-B show that the part of titanium excess η_e affects only maximal temperature and this practically does not change the combustion rate (curve 2 in *Fig. 2.b*).
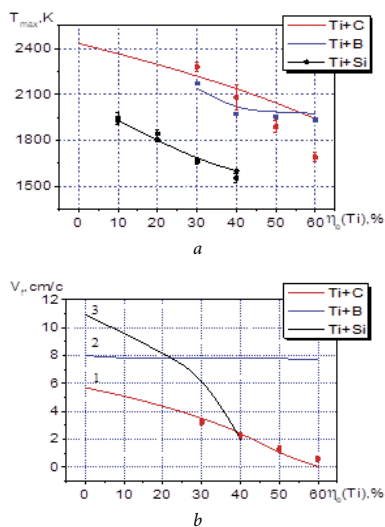
Fig. 2. *The dependencies of maximal temperature (a) and reaction front propagation (b) on the titanium excess in green mixture. $m_1=10$, $q_0=1.3$ MW/m^2 $m_2=10$; points – experimental data*

2. ábra *A nyers (zöld) keverékben a maximális hőmérséklet (a) és az reakció (égési) frontvonal terjedése (b) a titánban $m_1 = 10$, $q_0 = 1,3$ MW/m^2; kísérleti adatok $m_2=10$*

For various systems different combustion regimes were found. Typical qualitative picture for stationary combustion regime is presented in *Figs. 3.a* and *3.b.* for the system Ti+Si. For chosen composition, the reaction proceeds in the solid phase, melting temperature is not achieved. For $\eta_e=40\%$, the periodic regimes could be observed: after some reaction front delay, reaction can be renewed. This did not be observed for other systems. To demonstrate the difference in the combustion regimes, maximal temperature and average conversion versus time level are suitable. Average conversion level is calculated by the formula

$$\eta_\Sigma(t) = \frac{1}{(L-l)} \int_l^L \eta(x,t)dx .$$
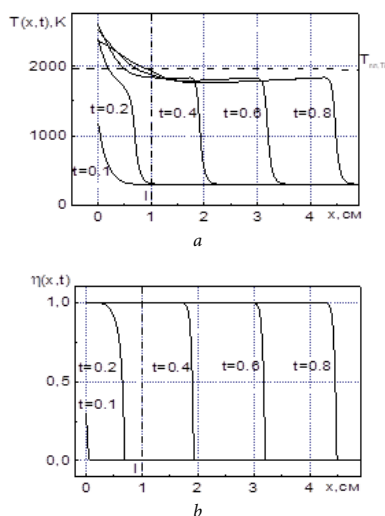
Fig. 3. *Temperature (a) and conversion level (b) for the stationary combustion regime. $\eta_e=20\%$; $q_0=1.3$ MW/m^2, system Ti+Si; time moments: t=1. 0.1; 2. 0.2; 3. 0.4; 4.0.6; 5. 0.8; 6.2.95 s*

3. ábra *A hőmérséklet (a) és a konverziós szint (b) stacionáris égési rendszer esetén a Ti-Si anyagrendszerben. $\eta_e = 20\%$; $q_0 = 1,3$ MW/m^2; idő pillanatok: t = 1. 0,1; 0,2; 3. 0,4; 4.0.6; 5,8; 6,2,95 s*
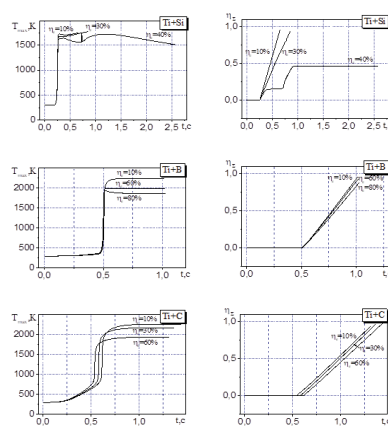
Fig. 4. *Maximal temperature and average conversion level versus time for various systems*

4. ábra *A maximális hőmérséklet és az átlagos konverziós szint az eltérő titán alapú anyagrendszerekben*

The results are presented in the *Fig. 4*. For the system Ti-Si (*Fig. 4.a*), practically stationary regimes with various rates are observed for η_e = 10 and 30%. Maximal temperature is not constant, the rate of the reaction front propagation can be determined as the slope of the curve $\eta_\Sigma(t)$. If η_e = 40%, the phenomena of the repeated reaction initiation takes place, but after $\eta_\Sigma(t) \approx 0,49$ reaction stops. Reaction front coordinate is presented in *Fig. 5* for various regimes. Quasistaionary regime with total conversion was found only for η_e = 10%. 5; for η_e = 80%, the repeated reaction initiation does not occur.

For the system Ti-B (*Fig. 4.b*), the quasistaionary regimes are characterized by different maximal temperatures. The reaction front rate determined as in [14] does not change; the reaction front rate determined as the slope of the curve $\eta_\Sigma(t)$ decrease very weakly. If η_e = 10%, maximal temperature grows slowly to stationary value when qusisiationary regime establishes; if η_e = 40%, combustion temperature reaches to maxima and then diminishes to stationary value.
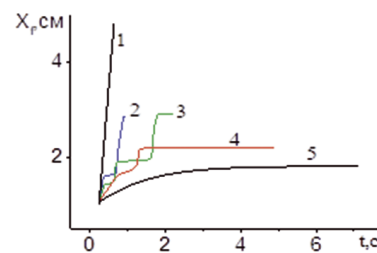
Fig.5. *Reaction front coordinate versus time for the system Ti-Si; $m_1=10$, $m_2=10$, $q_0=1.3$ MW/m^2 Curves: 1. 10%; 2. 40%; 3. 50%; 4. 60%; 5. 80%*

5. ábra *A reakció frontvonal terjedése az idő függvényében a Ti-Si rendszerben; $m_1=10$, $m_2=10$, $q_0=1,3MW/m^2$; Konverziós szintek:: 1. 10%; 2. 40%; 3. 50%; 4. 60%; 5. 80%*

For the system Ti-C (*Fig. 4.c*), the rize of titanium excess leads to the reaction zone expansion, quick maximal temperature decrease, however the reaction starts earlier. Reaction front rate decreases, if it is determined by the method [14], however it does not change, if it calculated as the slope of the curve $\eta_\Sigma(t)$. To understand the difference in the physical mechanism of the synthesis and the reaction front propagation the additional experimental and theoretical study are necessary.

4. Conclusions

So, the solid-phase combustion model with summary reaction scheme was realized numerically for three systems: titanium-carbon, titanium-boron, titanium-silicon. Taking into account nonstoichiometric composition of initial powder mixture, reaction retardation by reaction product, and dependence of properties on composition, the qualitative compliance between theory and experiment was obtained. The various combustion regimes for different systems were detected. Following study should include the detailed reaction scheme corresponding to irreversible conditions and porosity evolution during composite synthesis.

5. Acknowledgements

References

[1] Merzhanov, A. G. (2003): Combustion and explosion processes in physical chemistry and technology of inorganic materials. *Russian Chemical Reviews,* Vol. 72, No 4, 2003, pp. 289 – 310. https://doi.org/10.1070/RC2003v072n04ABEH000766

[2] Rogachev, Alexander S. – Mukasyan, Alexander S. (2015): Combustion for Material Synthesis, Taylor Francis Group, 424 P

[3] Mas-Guindal M. J., – Contreras, L. – Turrillas, X. – Vaughan, G.B.M. – Kvick, A. – Rodriguez, M. A. (2006): Self-propagating high-temperature synthesis of TiC–WC composite materials. *Journal of Alloys and Compounds*, Vol. 419, 2006, pp. 227–233 https://doi.org/10.1016/j.jallcom.2005.08.079

[4] Yang, Y. F. – Jiang, Q. C. (2013): Reaction behaviour, microstructure and mechanical properties of TiC–TiB2/Ni composite fabricated by pressure assisted self-propagating high-temperature synthesis in air and vacuum. *Materials and Design*, Vol.49 August 2013, pp. 123–129 https://doi.org/10.1016/j.matdes.2013.02.036

[5] Fra, E. – Janas, A. – Kolbus, A. – Olejnik, E. (2009): Cast in situ composites of Ni₃Al / MeC type. *Archives of foundry engineering*, Vol. 9, Is. 2. 2009. pp.81-86

[6] Ahmed, Y. M. Z. – Zaki, Z. I. – Bordia, R. K. – Besisa, D. H. A. – Amin, A. M. M. (2016): Simultaneous synthesis and sintering of TiC/Al₂O₃ composite via self propagating synthesis with direct consolidation technique, *Ceramics International,* Vol. 42, 15 November, 2016, pp.16589–16597 https://doi.org/10.1016/j.ceramint.2016.07.080

[7] Sutton, Austin T. – Kriewall, Caitlin S. – Leu, Ming C. – Newkirk, Joseph W. (2016): Powders for additive manufacturing processes: characterization techniques and effects on part properties - Solid Freeform Fabrication 2016: Proceedings of the 26th Annual International Solid Freeform Fabrication Symposium – An Additive Manufacturing Conference; The Department of Energy's Kansas City National Security Campus is operated and managed by Honeywell Federal Manufacturing Technologies, LLC under contract number DE-NA0002839. *Virtual and Physical Prototyping*, V. 12, 2017, Is. 1 pp.3-29

[8] Pribytkov, G. A. – Krinitcin, M. G. – Korzhova, V. V. (2016): Investigation of the products of SH-synthesis in powder mixture of titanium and carbon (in Russian), *Perspective materials,* 2016, №5, P. 59-68

[9] Strunina, A. G. – Firsov, A. N. – Kostin, S. V. (1981): Transition modes in the combustion of heterogeneous systems with solid-phase products, *Combustion, Explosion and Shock Waves,* 1981, V. 17, Is. 5, pp. 500–505 https://doi.org/10.1007/BF00798134

[10] Babichev, A. P. – Babushkina, N. A. – Bratkovskii, A. M. (1991): Physical values: reference book (in Russian), Grigoriev I.S., Meilikhova M. – eds. / M.: *Energoatomizdat*, 1991. 1232 pp.

[11] Yeh, C. L. – Chen, W. H. – Hsu, C. C. (2007): Formation of titanium silicides Ti5Si3 and TiSi2 by self-propagating combustion synthesis, *Journal of Alloys and Compounds,* 2007, Vol. 432, Is.1-2, pp. 90–95. https://doi.org/10.1016/j.jallcom.2006.05.131

[12] Capaldi, M. J. – Said, A. – Wood, J. V. (1997): Reaction Synthesis of TiC and Fe-TiC composites, *ISIJ International*, 1997,Vol. 37. № 2, pp. 188-193. https://doi.org/10.2355/isijinternational.37.188

[13] Kartal, G. – Timur, S. (2013): Growth kinetics of titanium borides produced by CRTD-Bor method. *Surface & Coatings Technology,* 2013, Vol. 215, pp. 440–446. https://doi.org/10.1016/j.surfcoat.2012.08.076

[14] Chumakov, Yu. A. – Knyazeva, A. G. – Pribytkov, G. A. (2017): Synthesis of the composites on the base of titanium in the combustion mode (in Russian), *Chemical physics and mesoscopy.* 2017, V.19, № 4. – pp.

Titán alapú kompozít szintézise égési rendszerben
Jelen munkában a szerzők numerikusan modelezik a karbid, borid és szilicid zárványokat tartalmazó titán alapú kompozit szintézisét. modellje numerikusan valósul meg. Feltételezik, hogy a fém titán többletet tartalmazó Ti-C, Ti-B és Ti-Si por-keverékek termikus szintetizálása során sztöchiometrikusan képződnek a TiC, TiB és Ti₅Si₃ komponensek – létrehozva ezáltal egy új kompozít anyagszerkezetet. Az általuk alkalmazott mődszer az „égető modellek" klasszikus ötletén alapszik, ahol a kémiai átalakulások és reakciók mint a „közvetlen égés" eredménye mennek végbe. Mindazonáltal az alkalmazott módszer figyelembe veszi a nyers (zöld) keverék nem-sztöchiometrikus összetételét, a tulajdonságok függé-sét a szintézis során változó összetételre és a gyújtóreakció kezdeti szakaszára. A hőmérséklet-eloszlást, a konverziós szintet, a maximális égési hőmérsékletet, a reakciózónák vastagságát és a reakció terjedésének sebességét numeri-kusan határozzák meg. A termék-hőmérséklet számítás kapott eredményei minőségi szempontból jól megegyeznek a mért kísérleti adatokkal.
Kulcsszavak: kompozit szintézis, nem-sztöchiometrikus keverék, gázmentes égés, reakciókésleltetés reakciótermék-kel, égés átmenet határfelületen

Voltammetric study of saffron in blood mediated by modified glassy carbon electrode (GCE) with carbon nanotube (CNT/GCE)

Muhammed Mizher Radhi ▪ Department of Radiological Techniques, Health and Medical Technology College-Baghdad, Middle Technical University ▪ mmradhi@yahoo.com

Maysara Samer Khalaf ▪ Department of Radiological Techniques, Health and Medical Technology College-Baghdad, Middle Technical University

Zainab Oun Ali ▪ Department of Radiological Techniques, Health and Medical Technology College-Baghdad, Middle Technical University

Thamir Aboud Al-Dabbagh ▪ Biomedical Engineering, University of Technology-Baghdad

Muhammed Mizher RADHI
Professor, Department of Radiological Techniques, Health and Medical Technology College-Baghdad, Middle Technical University, Baghdad, Iraq. He received his PhD from University Putra of Malaysia (UPM) in 2010 in Electrochemistry, Nanotechnology. Research topics: conductivity of grafted polymer with nano-deposit and fabrication of sensors by nanomaterials to study drugs in blood medium by electrochemical analysis.

Maysara Samer KHALAF
Lecturer, Department of Radiological Techniques, Health and Medical Technology College-Baghdad, Middle Technical University, Baghdad, Iraq. She received her PhD from College of Medicine, Department of Microbiology, Al-Nahrain University in Baghdad. Research topics: molecular biology.

Zainab Oun ALI
Lecturer, Department of Radiological Techniques, Health and Medical Technology College-Baghdad, Middle Technical University, Baghdad, Iraq. She received her PhD from College of Veterinary Medicine, University of Baghdad, Iraq. Research topics: surgery.

Thamir Aboud AL-DABBAGH
Assistant professor, Biomedical Engineering Dept., University of Technology-Baghdad, Iraq. He received his Master degree from College of Veterinary Medicine, University of Baghdad, Iraq. Research topics: anatomy and histology.

Abstract

Modified glassy carbon electrode with carbon nanotubes (CNT/GCE) was used to study extracted saffron in blood medium to find the effect of oxidation-reduction current peaks of saffron compound. It was found two cathodic current peaks at -0.75 and -1.75 V were appeared in the cyclic voltammogram of saffron in blood medium, so saffron considered as anti-oxidative compound in blood medium. Different concentrations, scan rates and effect of ascorbic acid on the cathodic current peak were studied. Diffusion coefficient of two reduction current peaks of saffron in blood medium was determined from Randel equations with values of saffron in blood medium at -0.75 and -1.75 V are 2.2×10^{-6} and 1.1×10^{-5} cm²/sec respectively cm² sec⁻¹.
Keywords:

1. Introduction

Saffron considered being an anti-oxidative reagent, especially in blood medium, which can be studied by electrochemical method using the cyclic voltammetric analysis. This method has been used recently through different research [1-6].

It was found that saffron effect on the blood pressure when use as nutrition. Saffron reduced the cross-section area, media thickness, and elastic lamellae number of the aorta. Nutritional saffron prevented BP increases and remodeling of the aorta in hypertensive rats [7]. Saffron has biological activities including antihumoral, cytotoxic, hypolipidemic, anti-inflammatory, etc. In comparison, cholesterol-fed, water-drinking rats had serum triglyceride (TG) levels equal to the rats fed a normal diet. The results of this study indicate that consumption of saffron can reduce serum cholesterol and TG levels in cholesterol-fed rats, suggesting that saffron may be useful in treatment of hyperlipidemia [8]. The chronic administration of saffron aqueous extract could reduce the mean systolic blood pressure (MSBP) in desoxycorticosterone acetate (DOCA) salt treated rats in a dose dependent manner. This compound did not decrease the MSBP in normotensive rats. The data also showed that antihypertensive effects of saffron did not persist [9]. The results demonstrate that while detecting the electroactive neurochemical norepinephrine in blood is more challenging than obtaining the same fast scan cyclic voltammetry (FSCV) measurements in a buffer solution due to biofouling of the electrode, it is feasible to utilize a minimally invasive FSCV electrode to obtain neurochemical measurements in blood [10]. Phenolic antioxidants are ranked by reducing strength and characterized for reversibility using cyclic voltammetry at a glassy carbon electrode. Phenolics with an ortho-diphenol group show a first oxidation peak close to 400 mV (vs. Ag/AgCl) in a model wine solution (12% ethanol, 0.033 M tartaric acid, adjusted to pH 3.6), with a linear concentration dependence below 0.01 mM. Dilution of white wines 10×, and red wines 400×, gave first oxidation peak currents in the 1.5 to 2.2 µA range and 1.9 to 3.4 µC of charge passed by 500 mV, producing values for the concentrations of phenolic antioxidants with low oxidation potentials in the wines. Further peaks in the cyclic voltammograms of the diluted wines correspond to classes of phenolics with higher oxidation potentials, providing a qualitative assessment of wine phenolics based on reducing strength [11].

In this work, saffron was studied in blood medium using modified glassy carbon electrode with carbon nanotubes (CNT/GCE) by cyclic voltammetric method.

2. Experimental

2.1. Reagents and chemicals

Saffron was supplied from EDMAN Company (Iran) as solid material which dissolved in deionized water after filtering by filter paper to use in the experiments. Blood samples were used from healthy human in Baghdad hospital center, and other chemicals and solvents were of annular grade and used as received from the manufacturer. Double distilled water was used for the preparation of aqueous solutions. All solutions were deaerated with oxygen free nitrogen gas for 15 min prior to making the measurement. All experiments were done at room temperature 25°C.

2.2. Preparing the modification of GCE with CNT (CNT/GCE)

Mechanical attachment technical method was employed to prepare the CNT/GCE working electrode as a nano-sensor [12,13]. The method of the modification of GCE included abrasive application of multiwall carbon nanotubes (MWCNT) on the clean surface of GCE, forming an array of MWCNT as modified working electrode MWCNT/GCE and replaced in 10 ml of electrolyte in the cyclic voltammetric cell, then connected all electrodes (working electrode, reference electrode and counter electrode) with the potentiostat.

2.3. Apparatus and procedures

Instruments: EZstat series (potentiostat/galvanostat) NuVant Systems Inc. pioneering electrochemical technologies USA Electrochemical workstations of Bioanalytical system with potentiostat driven by electroanalytical measuring software was connected to personal computer to perform Cyclic Voltammetry (CV), an Ag/AgCl (3M NaCl) and Platinum wire (1 mm diameter) was used as a reference and counter electrode respectively. The glassy carbon working electrode (GCE) was used in this study and cleaning the surface by polishing Alumina (BASi compony USA).

3. Results and discussion

3.1. Study different concentration of saffron in blood medium (calibration graph)
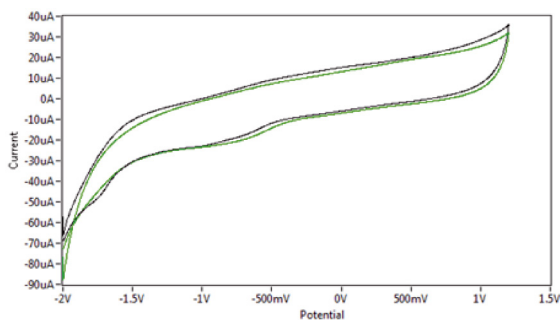
Fig. 1.   Cyclic voltammogram of saffron in blood medium at different concentration on CNT/GCE as working electrode versus Ag/AgCl as reference electrode at 100 mV sec^{-1}.
1. ábra   Sáfrány ciklikus voltammogramja vér közegben különböző koncentrációkban; mérő elektróda: CNT/GCE, referencia elektróda: Ag/AgCl, adatrögzítési sebesség: 100 mVsec^{-1}
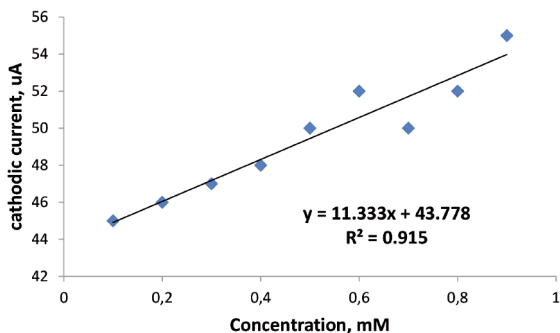
Fig. 2.   Plot of cathodic current peak at -1.75 V of saffron in blood medium against to different concentration.
2. ábra   Sáfrány különböző koncentrációi vér közegben; katódos áramerősség csúcsértékek -1.75 V feszültségnél

Fig. 1 shows the cyclic voltammogram of extracted saffron solution in blood medium at different concentration (0.1 - 0.5 mM). The two reduction current peaks of saffron in blood medium was appeared at potential -0.75 and -1.75 V and enhance to higher current against to increasing the concentration [14]. It was found the low detection limit of calibration graph as shown in *Fig. 2* with high sensitivity of the graph R²=0.915, by equation of Y=11.333X+43.778. These results were given a good indicator that the modified electrode CNT/GCE acts as electro-catalyst to detection of low concentration of saffron ions in blood medium [15].

3.2. Scan rate study

Different scan rate (0.01-0.1 V sec^{-1}) was studied for the saffron in blood medium as shown in *Fig. 3*. Also, it can be calculated the diffusion coefficient values of the cathodic current peaks by Randel equation [16]. *Fig. 3* illustrated the effect of different scan rate on the two reduction current peaks which enhance the current with increasing the scan rate and a good relationship between the reduction current peak at -0.75 V versus to the scan rate as shown in *Fig. 4*. A linear relationship was found from the equation of reduction peak is Y=153.28X+6.9013 with high sensitivity R²=0.9693, it means that the redox process of saffron compound in blood medium was reactant in homogeneous process [17].
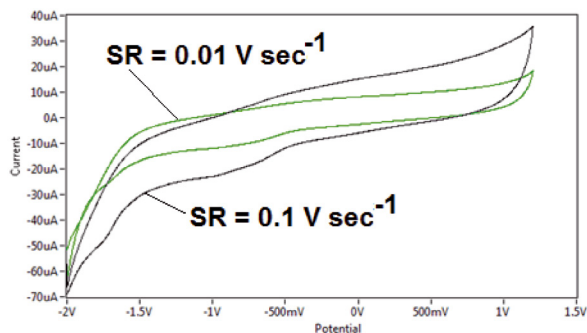
Fig. 3.   Cyclic voltammogram of saffron in blood medium at different scan rate (0.01-0.1 mV sec^{-1}) on CNT/GCE versus Ag/AgCl as reference electrode.
3. ábra   Sáfrány ciklikus voltammogramja vér közegben különböző adatrögzítési sebesség mellett (0.01-0.1 mV sec^{-1}); mérő elektróda: CNT/GCE, referencia elektróda: Ag/AgCl
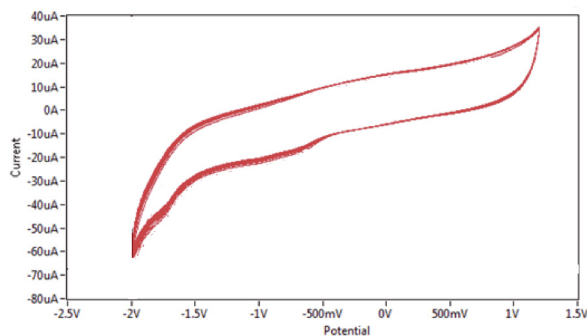
Fig. 4.   Plot of cathodic current peak at -1.05 V of saffron in blood medium against to different scan rate (0.01-0.1 V sec^{-1})
4. ábra   Sáfrány katódos áramerősség csúcsértékei vér közegben -1.05 V feszültségnél az atrögzítési sebesség függvényében (0.01-0.1 V sec^{-1})

3.3 Diffusion coefficient determination

The usual of mathematical method can be used in finding the diffusion coefficient of the redox process for the saffron compound in the KCl solution from the Randles-Seveik equation described reversible redox couple and the peak current [18,19].

$$I_p = (2.69 \times 10^5) \, n^{3/2} \, AC \, D_f^{1/2} \, v^{1/2} \qquad (1)$$

Where:

I_p is the current peak.

n is the number of moles of electrons transferred in the reaction.

A is the area of the electrode.

D_f is the diffusion coefficient.

V is the scan rate of the applied potential.

It was found the diffusion coefficient of two reduction current peaks at 0.75 and 1.75 V of saffron in blood medium are 2.2×10^{-6} and 1.1×10^{-5} cm²/sec respectively, the different in values attributed to the size of the ions which moving to the electrode through the blood medium [20].

3.4. Reliability and satiability study

Saffron compound in blood medium was study by modified of glassy carbon electrode with carbon nanotubes (CNT/GCE) in cyclic voltammetry. Ten times of scanning the cyclic voltammetry was studied as shown in *Fig. 5* and determination the relative standard deviation (RSD) for both reduction current peaks at -0.75 and -1.75 V of saffron with values are ± 1.3% and ± 1.5% respectively which has a good reliability and stability of saffron in blood medium with these results [21].

Fig. 5. Cyclic voltammogram of saffron in blood medium on CNT/GCE at ten times against to Ag/AgCl as reference electrode and at scan rate 100 mVsec⁻¹

5. ábra   Sáfrány ciklikus voltammogramja vér közegben CNT/GCE mérő elektródán tízszeres szorzóval Ag/AgCl referencia elektródához viszonyítva, 100 mV sec⁻¹adatrögzítési sebesség mellett

3.5. Effect ascorbic acid on the saffron in blood

Ascorbic acid (AA) is good anti-oxidative reagent especially in blood medium, but no effect of AA was appeared on the reduction peaks of saffron as shown in *Fig. 6* [22].
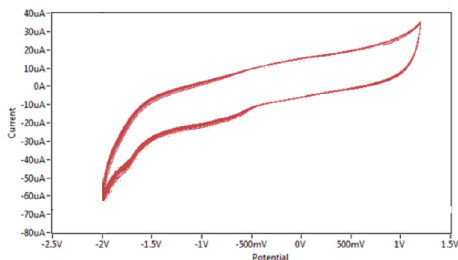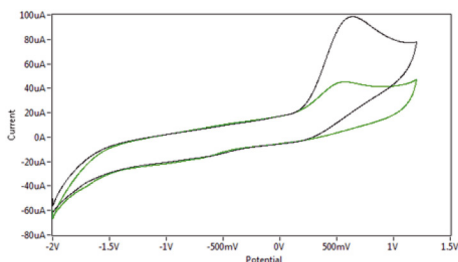

Fig. 6. Cyclic voltammogram of saffron compound with ascorbic acid in blood

medium at different concentration on CNT/GCE versus Ag/AgCl as reference electrode and scan rate 100 mV sec⁻¹.

6. ábra   Sáfrány ciklikus voltammogramja vér közegben különböző koncentrációkban aszkorbinsav jelenléte mellett; mérő elektróda: CNT/GCE, referencia elektróda: Ag/AgCl, adatrögzítési sebesség: 100 mVsec⁻¹

4. Conclusions

Saffron compound was extracted in aqueous solution was studied by cyclic voltammetric technique using modified glassy carbon electrode with carbon nanotubes to find the electrochemical behavior in blood medium and with ascorbic acid. It was found that saffron compound considered as anti-oxidative reagent in blood medium which appeared two cathodic current peaks in the cyclic voltammogram. Diffusion coefficient values of two reduction current peaks at -0.75 and -1.75 V were determined by Randel equation from different scan rate which has 2.2×10^{-6} and 1.1×10^{-5} cm²/sec respectively. The study was indicated that saffron compound is good antioxidant reagent in blood medium and there is no affected of ascorbic acid on the reduction current peaks of the saffron compound.

References

[1] Radhi, M. M. – Khalaf, M. S. – Ali, Z. O. et al. (2016): Voltammetric analysis of Zn (II) in present of each ascorbic acid (AA) and folic acid (FA) in human blood samples. *AASCIT Commus*, 2016, 3: 113-119.

[2] Abdul-Amir, Yousif Kadhim – Radhi, Muhammed Mizher – Al-Mulla, Emad Abbas Jaffar (2017): Use of Nano-Sensors of the Interferences between Pb((II) with Each of Mg(II), Zn(II), Mn(II), Ca(II), Co(II) and PO_4^{-3} in Blood Medium: An Electrochemical Study, *Nano Biomed. Eng.*, 2017, 9(3): 199-207. https://doi.org/10.5101/nbe.v9i3.p199-207

[3] Radhi, M. M. – Abdul-Amir, Y. K. – Khalaf, M. S. (2016): Electrochemical Effect of Acetylsalicylic Acid (Aspirin) in Present of Each Ascorbic Acid (AA) and Folic Acid (FA) in Normal Saline and Human Blood Samples, American Association for Science and Technology, *AASCIT Communications*, Vol. 3, No. 3, pp. 152-159.

[4] Radhi, M. M. – Al-Dulimy, W. G. – Khalaf, M. S. (2016): Electrochemical study of selenium (IV) mediated by carbon nanotubes modified glassy carbon electrode in blood medium, *Építőanyag-Journal of Silicate Based and Composite Materials*, Vol. 68, No. 3, pp. 90-93. https://doi.org/10.14382/epitoanyag-jsbcm.2016.16

[5] Radhi, M. M. – Abdullah, H. N. – Jabir, M. S. et al., (2017): Electrochemical effect of ascorbic acid on redox current peaks of CoCl2 in blood medium, *Nano. Bio. Eng.*, 2017, 9(2): 103-106. https://doi.org/10.5101/nbe.v9i2.p103-106

[6] Radhi, M. M. (2017): Voltammetric study of the redox current peaks of Pb(II) mediated by GCE in normal saline. *Am. J. Chem. Bio. Eng.*, 2017, 2(2): 26-34. https://doi.org/10.11648/j.ejb.20170503.11

[7] Nasiri, Zohreh – Sameni, Hamid Reza – Vakili, Abedin – Jarrahi, Morteza – Khorasani, Mahdi Zahedi (2015): Dietary saffron reduced the blood pressure and prevented remodeling of the aorta in L-NAME-induced hypertensive rats, *Iran J Basic Med Sci*. 2015 Nov; 18(11): 1143–1146.

[8] Thomson, Martha – Bou-Abbas, Fatima – Alansary, Abrar – Al-Qattan, Khaled K. – Ali, Muslim (2009): Effect of saffron on levels of blood lipids in rats fed a high cholesterol diet, *The FASEB Journal*, vol. 23 no. 1, 901-4, 2009.

[9] Imenshahidi, M. – Razavi, B. M. – Faal, A. – Gholampoor, A. – Mousavi, S. M. – Hosseinzadeh, H. (2013): The Effect of Chronic Administration of Saffron (Crocus sativus) Stigma Aqueous Extract on Systolic Blood Pressure in Rats. *Jundishapur J Nat Pharm Prod*. 2013 Nov; 8(4):175-9.

[10] Nicolai, E. N. – Trevathan, J. K. – Ross, E. K. – Lujan, J. L. – Blaha, C. D. – Bennet, K. E. – Lee, K. H. – Ludwig, K. A. (2017): Detection of Norepinephrine in Whole Blood via Fast Scan Cyclic Voltammetry. *IEEE Int Symp Med Meas Appl*. 2017 May;2017:111-116. https://doi.org/10.1109/MeMeA.2017.7985859

[11] Kilmartin, Paul A. – Zou, Honglei – Waterhouse, Andrew L. (2001): A Cyclic Voltammetry Method Suitable for Characterizing Antioxidant

Properties of Wine and Wine Phenolics, *J. Agric. Food Chem.*, 2001, 49 (4), pp 1957–1965. https://doi.org/10.1021/jf001044u

[12] Scholz, F. – Lange, B. (1992): Abrasive stripping voltammetry – an electrochemical solid state spectroscopy of wide applicability, *TrAC Trends in Analytical Chemistry,* Vol. 11, pp. 359-367 https://doi.org/10.1016/0165-9936(92)80025-2

[13] Tan, W. T. – Ng, G. K. – Bond, A. M. (2000): Electrochemical of microcrystalline tetrathiafulvalene at an electrode solid aqueous KBr interface, *Malaysian Journal of Chemistry,* Vol. 2, pp. 34-42.

[14] Sutter, Eli A. – Sutter, Peter W. (2014): Determination of Redox Reaction Rates and Orders by In Situ Liquid Cell Electron Microscopy of Pd and Au Solution Growth, *J. Am. Chem. Soc.*, 2014, 136 (48), pp 16865–16870. https://doi.org/10.1021/ja508279v

[15] Bard, A. J. – Faulkner, L. R. (2001): Electrochemical Methods: Fundamentals and Applications, 2nd Ed. *Wiley*, New York.

[16] Islam, Gazi Jahirul – Akhtar, H. M. Naseem – Mamun, M. A. – Ehsan, M. Q. (2009): Investigations on the redox behaviour of manganese in manganese(II)–saccharin and manganese(II)–saccharin–1,10-phenanthroline complexes, *Journal of Saudi Chemical Society* (2009) 13, 177–183. https://doi.org/10.1016/j.jscs.2009.05.002

[17] Bhatti, Naheed Kaukab – Subhani, M. Sadiq – Khan, Ather Yaseen – Qureshi, Rumana – Rahman, Abdur (2006): Heterogeneous Electron Transfer Rate Constants of Viologen Monocations at a Platinum Disk Electrode, *Turkish Journal of Chemistry.* 30 (2006) , 165-180.

[18] Zanello, P. (2003): Inorganic Electrochemistry: Theory, Practice and Application. *The Royal Society of Chemistry* 2003. https://doi.org/10.1039/9781847551146

[19] Crouch, Stanley R . – Skoog, Douglas A. (2006): Principles of instrumental analysis. *Cengage Learning* 2006.

[20] Cussler, E. L. (1997): Diffusion: Mass Transfer in Fluid Systems (2nd ed.). New York: *Cambridge University Press.*

[21] Torbeck, Lynn D. (2010): Statistical Solutions: %RSD: Friend or Foe, *Pharmaceutical Technology,* Volume 34, Issue 1, 2010.

[22] Haque, Farhana – Rahman, M. S. – Ahmed, Etmina – Bakshi, P. K. – Shaikh, A. A. (2013): Cyclic Voltammetric Study of the Redox Reaction of Cu(II) in Presence of Ascorbic Acid in Different pH Media, *Dhaka Univ. J. Sci.* 61(2): 161-166, 2013. https://doi.org/10.3329/dujs.v61i2.17064

Designing and Application of β-Cyclodextrin-based Copolymers for Remediation of Azo Dyes

Fatima TARIQ ▪ Department of Environmental Sciences, Fatima Jinnah Women University
▪ Fatimatariq86@gmail.com
Uzaira RAFIQUE ▪ Department of Environmental Sciences, Fatima Jinnah Women University

Fatima TARIQ Ph.D.
Ph.D scholar from Fatima Jinnah Women University, has completed her Ph.D. in 2018 with dissertation entitled "Development of hybrids as nanocarriers for targeted drug delivery". She also carried out applications of computational modelling on synthesized hybrids from University College London, UK. She has number of publications from her M.Phil and Ph.D research work. In addition she has file a patent along with the co-author of chapter based on various cinematographic techniques in manual.

Uzaira RAFIQUE
Dean of Faculty of Sciences and Technology at Fatima Jinnah Women University, Rawalpindi Pakistan. Her research expertise based on synthesis, structure and physical properties of inorganic, organic, hybrid and composite materials. The basic aim of her research group is to discover new materials with potential useful properties particularly with projected applications in field of environmental remediation.

Abstract

The world is facing pollution challenges globally and there is need to implement clean and cost-effective technologies to remediate the environment. The plan of present research work is to copolymerize synthetic materials (β-Cyclodextrin) as cost effective and eco-friendly adsorbents for environmental remediation. The synthetic material is copolymerized and further modified with beetroot peels. The samples were investigated under FTIR and SEM. The frequencies were recorded at 2931 cm^{-1} and 1016 cm^{-1} confirm the presence of β-Cyclodextrin in the synthesized copolymer. The wider cavities depicted under SEM are expected to enhance the uptake capacity of modified copolymers for organic moieties. The inclusion complex of β-Cyclodextrin depicts rectangular features with milky white surface confirmed by XRD. The synthesized copolymer was applied as adsorbent in a batch mode to determine efficiency for the amputation of a wide range of environmental pollutants. The results of UV-Vis have proved that Crystal violet and Congo red show (87%) and (69%) removal, respectively at optimum dose. The study concludes the successful synthesis of β-Cyclodextrin modified with beetroot peels as efficient adsorbent for the removal of dyes.

Keywords: β-Cyclodextrin, Crystal violet (CV), Congo red (CR), SEM, FTIR

1. Introduction

Rapid economic development due to increased industrial activities is a great challenge for the global world. The reason is lack of economical and eco-friendly remediation technologies for environment. Among variety of physio-chemical processes, adsorption technique [5] marks its distinction due to the communal mechanism for the removal of organic and inorganic pollutants from the environment. Mostly organic pollutants are of great concern due to their toxicity, persistence and bioaccumulation in living organisms [20]. It is alleged that eco-balance is disturbed due to the disposal and discharge of toxic and noxious pollutants by industries such as textile, leather, food and paint [12]. It is proposed that extensive applications of azo dyes in food, tanning, paper and textile at elevated level dissuade the attention of researchers towards the control of dyes by designing structures or materials from both eco-friendly and economical sources [13]. It is known that synthesis of adsorbents from natural [4] and synthetic sources can be employed as inexpensive approach but it defines certain limitations when they are used as adsorbent for environmental processes [11]. Present study was conducted to reduce the azodyes burden from environment by synthesizing β-Cyclodextrin based copolymers [8]. This new product exhibit exclusive properties such as high adsorption capacities due to the formation of inclusion complexes through host guest interactions. These interactions are responsible for the removal of toxic inorganic and organic moieties even at trace level [23].

2. Materials and methods

The materials β-Cyclodextrin, pyridine and ethanol were the reagents used for synthesis and purchased commercially from Sigma Aldrich. Apparatus included a UV-Vis spectrophotometer (SCHIMADU-1403).

2.1. Synthesis of β-Cyclodextrin based copolymer

The present protocol is based on synthesis of copolymers from waste sources to use as efficient adsorbents for the removal of environmental pollutants (azo dyes). In the preliminary tread, β-Cyclodextrin (60 mg) [22] was dissolved in 75 ml of pyridine and heated at 70⁰C. Beetroot peels (28 mg) and acetic acid (25 ml) were added and stirred in above mixture. Brown yellow solid crystals formed after 30 minutes. The mixture was washed successively with distilled water and ethanol. The beetroot modified β-Cyclodextrin based synthesized co-polymer is coded as CCD. Modification of copolymer with beetroot peels is reported for the first time in the present research. Direct co-condensation approach is adopted for the synthesis of copolymers, as this process is easier, convenient and efficient [7]. The objective of modification is to enhance the removal efficiency of synthesized co-polymer [9]. The copolymer before and after modification with beetroot peels is subjected to different characterization techniques.

3. Characterization

The synthesized material is subjected to following characterization techniques such as FTIR (Fourier Transform

Infrared (FTIR-8400 Schimadzu, Japan) spectrophotometer, XRD (STOE) and SEM (JEOL tsm-6490, Japan).

3.1 FTIR

The recorded FTIR spectrum of β-Cyclodextrin Copolymer is shown in *Fig. 1*. The peaks at 2932-3364 cm^{-1} identify the presence of N–H and O–H stretching in raw beetroot (also observed by [3] while peaks characteristics of β-Cyclodextrin are observed at 1033 cm^{-1} and 1357cm^{-1}). The peaks are assigned to anti-symmetric stretching of C-O-C and vibrational stretching of –C=C–, duly supported by [10]. The modification of β-Cyclodextrin with beetroot peels resulting in modified copolymer is confirmed by the peak observed at 1697 cm^{-1}. In addition, the peak at 2960.83 cm^{-1} [28] indicates the presence of Hydrogen free -NH-COO-,-NH$_2$- and –COOH groups in the modified co-polymer.
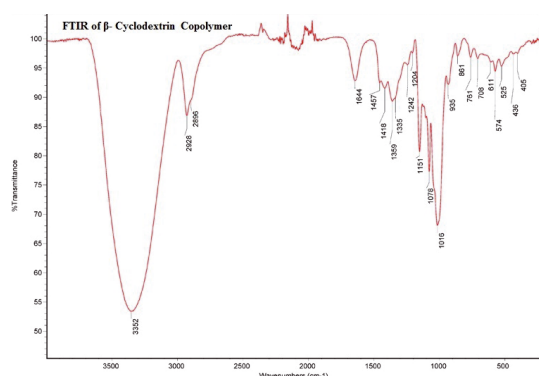
Fig. 1. FTIR spectrum of β-Cyclodextrin Copolymer
1. ábra β-ciklodextrin kopolimer FTIR spektruma

3.2 SEM

The surface morphology of beetroot peels, β-Cyclodextrin, and the modified copolymer synthesized is investigated under scanning electron microscopy. The images are shown in *Figs. 2.a* to *2.c*.

B-Cyclodextrin shows a regular surface with no intruding pores. However, the larger particles are scattered and overlaid with smaller particles. The beetroot peels depict a lump of aggregates with lamellar and non-homogenous surface (see *Fig. 2.b*). In addition, few crevices are also visible in the larger aggregate of beetroot.

The synthesis of copolymer can be easily followed in SEM images. The modification of β-Cyclodextrin and beetroot peels is witnessed as formation of continuous layer of β-Cyclodextrin as base film with beetroot modification on the surface. This modification is also accompanied with formation of new clearly distinct channels with defined pore volume (see *Fig. 2.c*). This indicates the change in surface morphology of the individual entities of β-Cyclodextrin and beetroot peels into a modified copolymer. The modification also favours the binding ability of β-Cyclodextrin with the guest molecules [16]. The development of channels in the modified copolymer is expected to act as adsorbent sites for the incoming pollutants to enhance the host-guest interactions of the inclusion complex [2].

3.3 XRD

The structure of the modified copolymer synthesised from β-Cyclodextrin and beetroot peels is predicted from XRD analysis. The XRD diffractogram (shown in *Fig. 3*) reveals the amorphous nature of the copolymer. The diffraction pattern with low intensity of 15.660 at 2θ [11] also indicate grain structure of synthesized material. The halo-diffused pattern for entirely amorphous copolymer of cyclodextrin was also identified by [17].
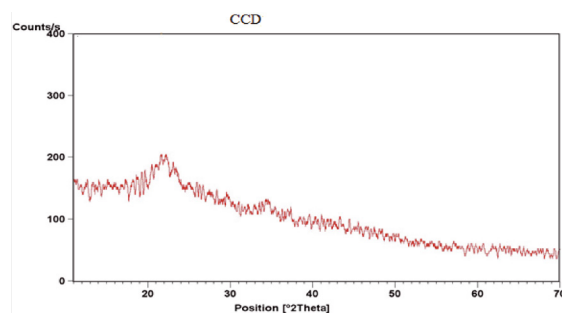
Fig. 3. XRD of synthesized β-Cyclodextrin modified beetroot peels copolymer
3. ábra A cékla héjjal módosított β-ciklodextrin kopolimer röntgendiffraktogramja
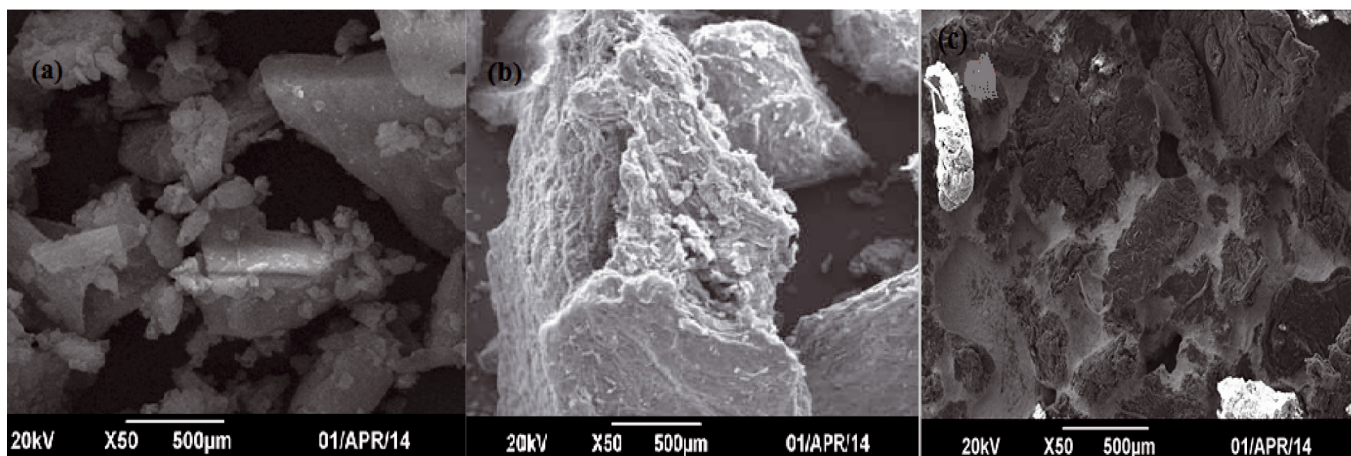
Fig. 2. SEM images of (a) β-Cyclodextrin (b) Beetroot peels (c) modified copolymer
2. ábra Pásztázó elektronmikroszkópos felvételek (a) β-ciklodextrin (b) cékla héj (c) módosított kopolimer

3.4 Batch adsorption experiment

A closed batch approach is adopted to investigate the adsorption capacity of synthesized copolymer as an adsorbent for the removal of dyes. The absorbance of Crystal violet and Congo red was recorded on UV-Visible spectrophotometer at λ max of 590 nm and 497 nm, respectively. Batch experiment was applied at variable adsorbent dosages (1 mg, 10 mg, 20 mg) and induced dye concentrations (0.01 mg/L, 0.03 mg/L and 0.05 mg/L).

The synthesized modified copolymer is applied as adsorbent for the removal of the selected dyes in a batch mode as a function of time. The results are graphically presented in *Figs. 4.a* and *4.b*. It is observed that the synthesized modified copolymer shows successive removal of Crystal violet and Congo red and continues till dynamic equilibrium [30] is attained in 25-30 minutes of contact. The incremental increase indicates that the process is non-linear and involves more than one step. Each step is operative independent of each other. However, the relatively rapid initial uptake is due availability of more vacant pores. The optimum removal of Congo red (67%) is relatively more than Crystal violet (59%). This suggests that the surface of the adsorbent has more susceptibility for the earlier likely due to acidic nature of Congo red showing stronger bonding to extensive –OH groups available on the surface of β-Cyclodextrin. Maxima of adsorption is followed by desorption partly due to saturation of sites and repulsive forces between the solute molecules [21] and groups of the synthesized adsorbent. The adsorption mechanism of modified copolymer is proposed to involve film diffusion and intra-particle diffusion simultaneously [24].
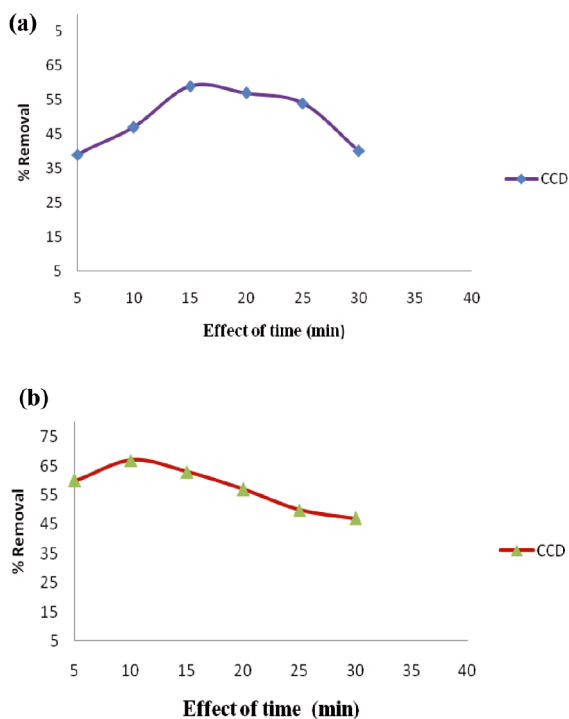
Fig. 4. Removal (in %age) of (a) Crystal violet (b) Congo red on synthesized copolymer as a function of time
4. ábra Indikátorok átcsapása a szintetizált kopolimerben a hatásidő függvényében (a) kristályibolya, (b) Kongóvörös

3.5 Effect of dose

The amount of adsorbent is varied to determine the effect of dose on the removal capacity. In the present investigation, dose of 1mg/Kg, 10mg/Kg and 20mg/Kg is applied for the removal of dyes. The results are graphically presented in *Figs. 5.a* and *5.b*. It is generally understood that as the dose increases, the adsorption sites are expected to increase and thus the adsorption potential [29]. Elevated increase in adsorption potential commensurate with the increase in adsorbent dose. This is equally good for the removal of both Congo red and Crystal violet. It justifies increasing surface area and availability of more exchange sites on the surface of adsorbents as supported by [18].
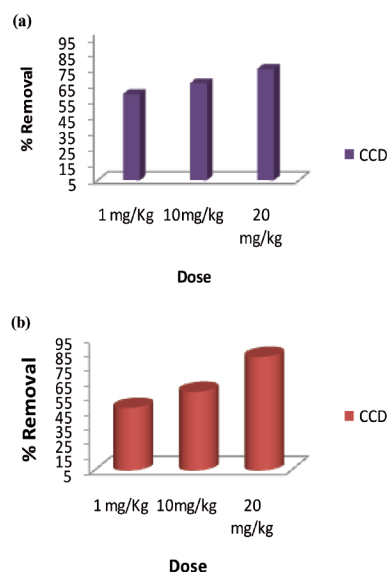
Fig. 5. Removal (in %age) of (a) Crystal violet (b) Congo red on synthesized copolymer as a function of dose
5. ábra Indikátorok átcsapása a szintetizált kopolimerben az adagolás függvényében (a) kristályibolya, (b) Kongóvörös

3.6 Effect of Concentration

The dye concentration is an important parameter to define the threshold for the uptake on the surface of adsorbent. The synthesized modified copolymer is tested against induced dye concentration of 0.01mg/L, 0.03mg/L, and 0.05mg/L. The results are graphically presented in *Figs. 6.a* and *6.b*. A regular increase in removal percentage of Crystal violet [19] is observed upon exposure of higher concentration of dye. More is the induced concentration of dye; more is the uptake of the dye on fixed dose of modified copolymer. The increase in initial concentration is likely to enhance interaction between adsorbent and dye. Similar results are observed by other researchers for dye uptake on adsorbents like activated carbon [27], carbon nanotube [25], oak sawdust [1], rice husk [26] cashew nut shell [14].

The augmented adsorption with increase in induced concentration may be attributed to complete mass transfer between the aqueous and solid phase of the dye molecules [16]. This reflects that the process of adsorption between the exposed concentration and adsorbent dose is continued and the spaces are still available for the uptake of more dye.

However, relatively less adsorption potential also suggests that removal is a slower and relatively less efficient process for Crystal violet [6].

On the contrary, Congo red shows more (86%) and faster (10 minutes) adsorption on modified copolymer. Furthermore, a maximum of removal (86%) is found at induced concentration of 0.03mg/L defining the optimum.

A decline in adsorption on further increase in concentration (see *Fig. 6.b*) suggests that the sites are being vacated after attaining saturation of congo red. This may be explained that mono ionic layer is formed at low concentration over the adsorbent surface [15]. The proposed mechanism may conclude that adsorption of Congo red and Crystal violet is governed by physicochemical and physical adsorption, respectively [19].
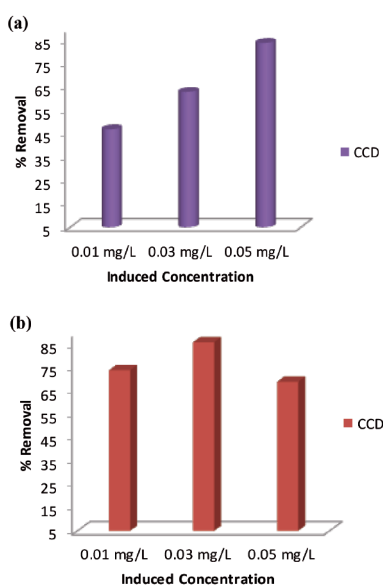

Fig. 6.   Removal of dyes (a) Crystal violet (b) Congo red as a function of induced concentration
6. ábra   Indikátorok átcsapása a szintetizált kopolimerben a koncentráció függvényében (a) kristályibolya, (b) Kongóvörös

4. Conclusions

The following conclusions can be drawn from the present research work:

The method adopted provides an efficient, easy and an innovative greener approach towards modification of β-Cyclodextrin with natural source of beetroot peels.

The synthesized copolymer is proven to be a good and efficient adsorbent for the removal of toxic azo dyes (Congo red, Crystal violet) from aqueous environment under varying parameters.

The study provides a good and cheaper alternate to commercial and expensive adsorbents.

It recommends the commercial viability of synthesized modified copolymer for in-situ remediation of industrial pollutants.

References

[1] Ei-latif, M. M. Abd – Ibrahim, A. M. – Kady, M. F. E. I. (2010): *J. Am. Sci* Vol. 6 pp. 267-283.

[2] Ansari, R. – Seyghali, B. – Khah, M. A. (2012): *Journal Surfact Deterg* Vol 15 pp. 557–565. https://doi.org/10.1007/s11743-012-1334-3

[3] Bao, J. Y. – Wen, C. D. (2013): *Chinese Journal of Analytical Chemistry* Vol. 41 No. 8 pp. 1264-1268. https://doi.org/10.1016/S1872-2040(13)60675-1

[4] Barikani, M. – Mohammadi, M. (2007): *Carbohydrate Polymers* Vol. 68 pp. 773–780. https://doi.org/10.1016/j.carbpol.2006.08.017

[5] Browski, D. (2001): *Advances in Colloid and Interface Science* Vol. 93 pp. 135-224.

[6] Crini, G. (2005): *Progress in polymer science and thermodynamic study* Vol. 30 No. 1 pp. 38-70. https://doi.org/10.1016/S0001-8686(00)00082-8

[7] Da'na, E. – Sayari, A. (2011): *Chemical Engineering Journal* Vol. 166 No. 1 pp. 445-453.

[8] Dhodapkar, R. – Borde, P. – Nandy, T. (2009): *Global Nest Journal* Vol. 11 No. 2 pp. 223-234. https://doi.org/10.1016/j.cej.2010.11.016

[9] Fatima, T. – Uzaira, R. (2015): *International Journal of Innovation and Scientific Research* Vol. 13 No. 2 pp. 485-496.

[10] Gidwani, B. – Vyas, A. (2014): *Colloids and Surfaces B: Biointerfaces* Vol. 114 pp. 130-137. https://doi.org/10.1016/j.colsurfb.2013.09.035

[11] Jiang, H. – Zujin, A. N. G. – Xiantai, H. O. U. (2012): *Chinese Journal of Chemical Engineering* Vol. 20 No. 4 pp. 784-792. https://doi.org/10.1016/S1004-9541(11)60249-8

[12] Julinova, M. – Slavik, R. (2012): *Journal of Environmental Management* Vol. 94 pp. 13-24. https://doi.org/10.1016/j.jenvman.2011.09.006

[13] Khatoon, L. N. – Khan, H. A. – Pathak, V. (2013): *International Journal of Innovative Research in Science, Engineering and Technology* Vol. 2 No. 11 pp. 2319-8753.

[14] Kumar, S. – Ramalingam, S. – Senthamarai, C. (2010): *Desalination*, Vol. 261 pp. 52-60. https://doi.org/10.1016/j.desal.2010.05.032

[15] Nidheesh, P. V. – Gandhimathi, R. – Ramesh, S. T. (2012): *Turkish Journal of Engineering and Environmental Sciences* Vol. 36 No. 3 pp. 249-262. https://doi.org/10.3906/muh-1110-3

[16] Norasiha, H. (2011): *PhD Thesis, University of Malaysia Pahang*

[17] Parkpain, P. – Sreesai, S. – Delaune, R. D. (2014): *Water, Air and Soil Pollution* Vol. 122 pp. 163-182. https://doi.org/10.1023/A:1005247427037

[18] Patil, A. K. – Shrivastava, V. S. (2010): *International Journal of Chem Tech Research* Vol. 2 No. 2 pp. 842-850.

[19] Patil, M. S – Deshmukh, V. – Renukdas, S. (2011): *International Journal of Environmental Sciences* Vol. 1 No. 6 pp. 0976 – 4402.

[20] Pentyala, N. S. – Rebecchi, M. – Mishra, S. (2011): *Environment. Polluiont. Ecological. Human. Health* Vol. 23 pp. 249-262.

[21] Priya, R. – Nithya, R. – Anuradha, R. (2014): *International Journal of Chem Tech Research* Vol. 6 No. 9 pp. 4346-4351.

[22] Rima, J. – Assaker, K. (2013): *Inorganic Contaminants from Water* Vol. 2 No. 1 pp. 887-895. https://doi.org/10.5539/jfr.v2n1p150

[23] Sambasevam, P. K. – Mohamad, S. – Sarih, M. N. (2013): *International Journal Mol. Science* Vol. 14 pp. 3671-3682. https://doi.org/10.3390/ijms14023671

[24] Sen, T. K. – Afroze, S. – Ang, H. (2011): *Water, Air, & Soil Pollution* Vol. 2 No. 18 pp. 499-515. https://doi.org/10.3390/ijms14023671

[25] Shahryari, Z. – Goharrizi, A. S. – Azadi, M. (2010): *Int. J. Water Resour. Environ. Eng* Vol. 2 pp. 16–28.

[26] Sharma, P. – Kaur, R. – Baskar, C. (2010): *Desalination*, Vol. 259 pp. 249-257. https://doi.org/10.1016/j.desal.2010.03.044

[27] Sharma, Y. C. (2009): *Journal of Chemical & Engineering Data* Vol. 55 pp. 435-439. https://doi.org/10.1021/je900408s

[28] Stalin, T. – Srinivasan, K. – Sivakumar, K. (2014): *Journal of Molecular Structure* Vol. 106 pp. 239–250. https://doi.org/10.1016/j.molstruc.2013.11.048

[29] Vanitha, T. (2014): *International Research Journal of Advanced Zoology, Animal Science and Nutrition (SIRJ-AZASN)* Vol. 1 No. 1 pp. 2349 – 4263.

[30] Wanyonyi, C. W. – Onyari, M. J. – Shiundu, M. P. (2014): *Energy Procedia* Vol. 50 pp. 862 – 869. https://doi.org/10.1016/j.egypro.2014.06.105

Heat effected zone in unburned, antimony trioxide containing plasticised PVC

Ali I. AL-MOSAWI
PhD student in Polymers Engineering Department, Faculty of Materials Science and Engineering, University of Miskolc, Hungary. M.Sc. and B.Sc. in Materials Engineering, Faculty of Engineering, Babylon University, Iraq. Research Interests: Polymers, Composite Materials, Rubber Technology, Flame Retardants, Materials Testing, Materials Processing.

Ali I. AL-MOSAWI ▪ University of Miskolc, Hungary ▪ qkoali76@uni-miskolc.hu
Kálmán MAROSSY ▪ University of Miskolc, Hungary ▪ polkal01@uni-miskolc.hu

Kálmán MAROSSY
Professor of Polymer Engineering at Institute of Ceramic and Polymer Engineering, University of Miskolc, Hungary. Recent Research Interests: Polymer Blends, Multiphase Polymer Systems, Relaxation Phenomenon, Polymer Degradation, Composite Materials, Rubber.
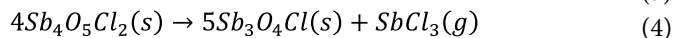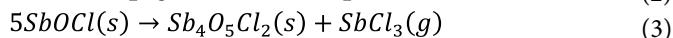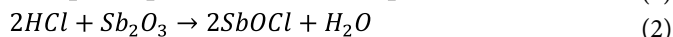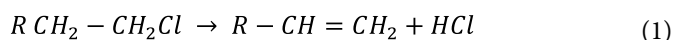
Abstract

What are the structural changes in the PVC layer located directly under the flame zone which is exposed to high temperatures without burning? We will try to explain in this article what actually happens in this layer, which we called heat affected zone. The layers were tested both with and without antimony trioxide (ATO or Sb_2O_3) flame retardant additive. Results obtained from Scanning electron microscopy (SEM) for the heat affected zone of the samples after Limited oxygen index (L.O.I.) test and compared with the samples before this test showed that there was a significant decrease in the chlorine content in the PVC structure accompanied by a significant increase in the carbon content. We suppose that this early dehydrochlorination improves the efficiency of Sb_2O_3.
Keywords: Plasticised PVC, HAZ, L.O.I., SEM, EDS

1. Introduction

The process of flame retardancy doesn't relate to the material's melting temperature itself, but depending only on the metaphase transformations that grow inside the material, as well as depends on compounds consisting after exposure retardant material to high temperatures. For instance, ceramic materials make a full thermal insulation due to the poor thermal conductivity but not necessarily resist flame, even if the high degrees of melting. The fire-inhibiting materials are on the contrary, they are in degrees of heat is one of the low-lying conductive materials, but at high flame is a good heat insulators in addition to immunity to flame spread [1]. Antimony trioxide is not considered a flame retardant when it is added to low-flame-resistant materials, but it is used to increase the flame retardant effect of halogen flame retardants if added to different proportions and as needed to improve its flame resistance performance [2-7]. When the polymer contains halogen flame retardants with antimony trioxide is exposed to flame, the antimony trioxide starts by interacting with the chlorine from the polymer, and chemical compounds such as $SbCl_3$ SbOCl will be formed which neutralize the free radicals, kill the flame and prevent its spread. This reaction mechanism is described in the equations as follows [8-12]:

$$R\ CH_2 - CH_2Cl \rightarrow R - CH = CH_2 + HCl \quad (1)$$
$$2HCl + Sb_2O_3 \rightarrow 2SbOCl + H_2O \quad (2)$$
$$5SbOCl(s) \rightarrow Sb_4O_5Cl_2(s) + SbCl_3(g) \quad (3)$$
$$4Sb_4O_5Cl_2(s) \rightarrow 5Sb_3O_4Cl(s) + SbCl_3(g) \quad (4)$$
$$3Sb_3O_4Cl(s) \rightarrow 4Sb_2O_3(s) + SbCl_3(g) \quad (5)$$

s = solid; g = gaseous

Eq. (1) was extended for the better representation of the reaction. However, when the antimony trioxide is added to PVC it becomes very effective to flame retarding, because it acts as a synergist for the halogen contained inherently in the

PVC (56.7%). This situation is similar to that obtained from the stimulation of halogen flame retardants and the same compounds will be formed when ATO reacts with chlorine released from the PVC after it is burned [13-16].

2. Materials and methods

a. Materials: PVC S-5070 (Ongrovil`) from BorsodChem Zrt., Hungary; Dioctyl Phthalate (DOP) as plasticizer; Newstab 50 as stabilizer; Wax-E as lubricant; and antimony trioxide (ATO) with chemical formula Sb_2O_3.

b. Sample preparation: four batches were prepared with a laboratory extruder (Göttfert Extrusiometer G20) at 170 ºC. The barrel diameter is 20 mm, the length 20D, i.e. 400 mm. A screw of comparison rate was used with long comparison zone (PVC screw). The die was 10×4 mm flat die suitable for extruding rods for L. O. I. test without further forming.

c. Thermal tests: Limiting oxygen index test (L. O. I.) was done by the instrument Stanton Redcroft FTA flammability unit with oxygen and nitrogen cylinders gas and accurate pressure control system found in BorsodChem Zrt. The results obtained from this test shown in *Fig. 1*. As expected, we can observed from this figure that the limiting oxygen index of PVC increased with ATO additions, This increase is direct, as the percentage of ATO increased the value of L. O. I. will increase. Also, the percentage of oxygen which the PVC samples needs to burn will increase. This behavior due to the ATO absorbed heat and there will be phase transformations in its internal structure. This represent endothermic process which decreased surface temperature which will prevent fire propagation [4,13].
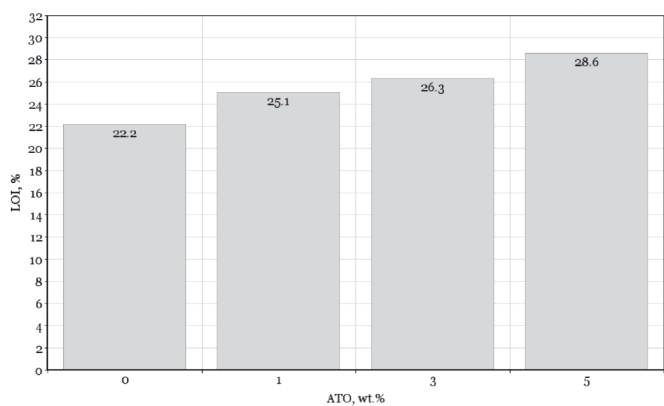
Fig. 1.   Limiting oxygen index of plasticised PVC vs. ATO additives
1. ábra   ATO tartalmú lágyított PVC oxigén indexe

d. Scanning electron microscopy FESEM: FESEM was used for the structural analysis of plasticised PVC. This test was done by using Carl Zeiss EVO MA10 SEM.

e. Thermal gradient: thermal imaging camera (FLIR Systems) was used in order to determine the thermal gradient in L. O. I. test samples as shown in *Fig. 2*. The Emissivity was 0.5, reflected apparent temperature 20°C, and Object distance 1.0 m
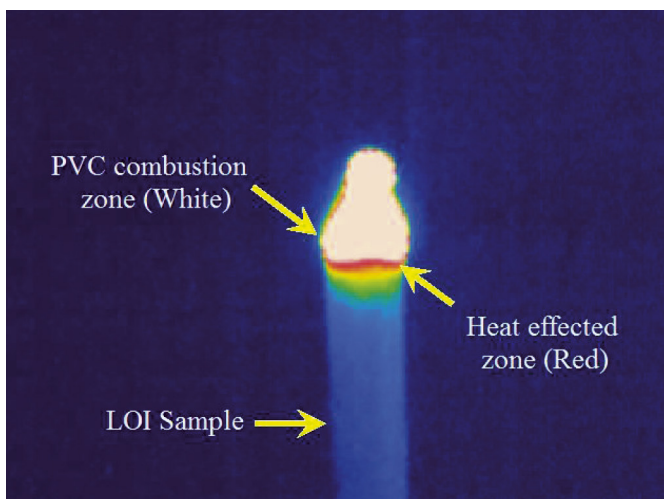
Fig. 2.   FLIR thermal gradient image for heat affected zone (HAZ) in plasticised PVC L. O. I. test
2. ábra   A hőhatásnak kitett zóna (HAZ) FLIR termikus gradiens képe a lágyított PVC L. O. I. vizsgálata közben

3. Results and discussion

The images obtained from SEM show that the chlorine percentage decreased associated with an increase in carbon percentage after L. O. I. test, when comparing with PVC SEM images before the test, as shown in *Fig. 3* and *Fig. 4*. This state as a result of PVC dehydrochlorination, where it begins to release chlorine in form of HCl from its internal structure at high temperatures, i.e. begins to decompsion in these tempreature. The loss of chlorine from the internal structure of PVC involves not only burnt and directly exposed layers of fire, but also extends to the under layers far from the combustion zone, which we called heat affected zone (HAZ) as shown in figures.

In addition, we noticed that the under layers of the test samples ignite faster when cutting the burned area and continue the L. O. I. test, which means the low flammable resistance for heat affected layer because less chlorine. However, this situation soon changes and PVC resistance to ignition improves after the addition of the antimony trioxide as shown in *Figs. 5-7*, where the released chlorine will be reduced from the heat affected zone. It is true that the antimony trioxide alone is not a flame retardant but it improves and increases flame retardation if it is added to halogen-containing flame retardant material containing chlorine. Antimony trioxide and chlorine combine compounds that have the ability to inhibit flame and improve flame resistance. While the structure of PVC contains a chlorine, it begins to release as a result of combustion and thermal decomposition. This chlorine reacts with the antimony trioxide forming $SbCl_3$ compound [17], which help to reduce PVC combustion and increase heat resistance of the heat affected zone. After the addition of antimony trioxide, the heat affected layer ignites relatively slowly when the burnt area is cut and the L. O. I. test continues, which means high flame resistance of this layer. The efficient flame retardant is the $SbCl_3$ is already prepared in the heat affected zone, therefore the extinguishing of the falme starts sooner.
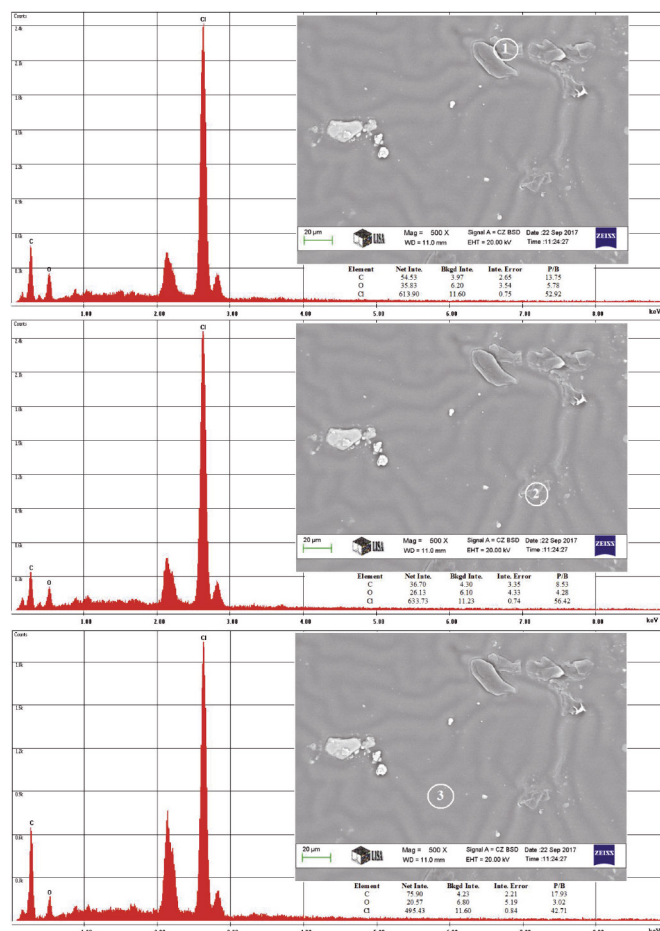
Fig. 3.   SEM - energy dispersive X-ray microanalysis for unburned plasticised PVC
3. ábra   SEM - energia diszperzív röntgen mikroanalízis az el nem égett PVC-ben

Fig. 4. SEM - energy dispersive X-ray microanalysis for HAZ in burned plasticised PVC L. O. I. sample

4. ábra SEM - energia diszperzív röntgen mikroanalízis HAZ esetében az elégett lágyított PVC L. O. I. mintában

Fig. 6. SEM - energy dispersive X-ray microanalysis for HAZ in burned plasticised PVC + 3% Sb_2O_3 LOI sample

6. ábra SEM - energia diszperzív röntgen mikroanalízis a HAZ az elégetett lágyított PVC-ben. Sb_2O_3 tartalom 3%

Fig. 5. SEM - energy dispersive X-ray microanalysis for HAZ in burned plasticised PVC + 1% Sb_2O_3 LOI sample

5. ábra SEM - energia diszperzív röntgen mikroanalízis a HAZ az elégetett lágyított PVC-ben. Sb_2O_3 tartalom 1%

Fig. 7. SEM - energy dispersive X-ray microanalysis for HAZ in burned plasticised PVC + 5% Sb_2O_3 LOI sample

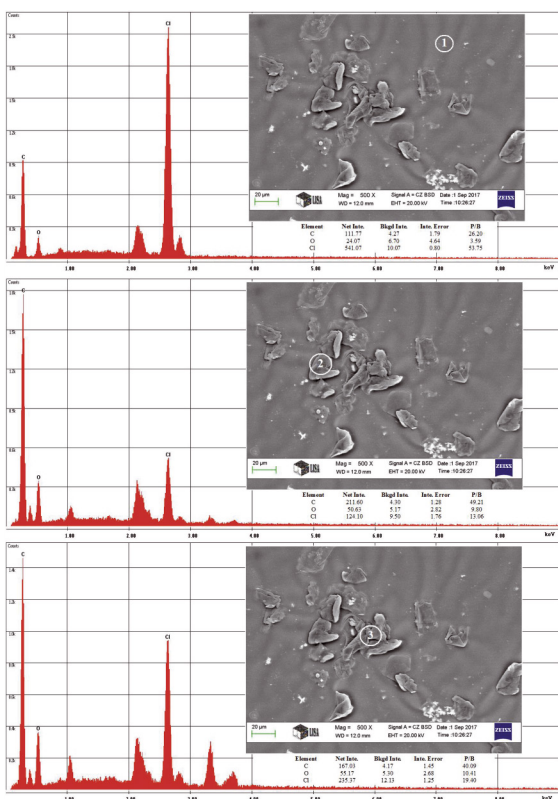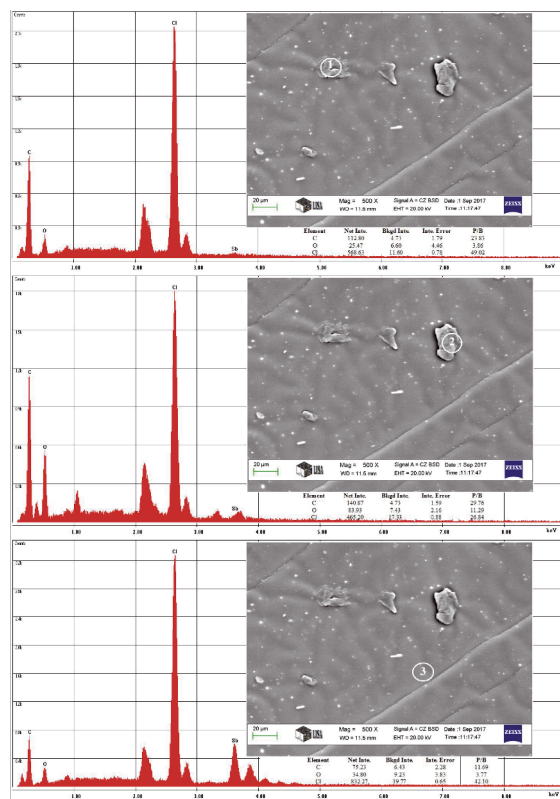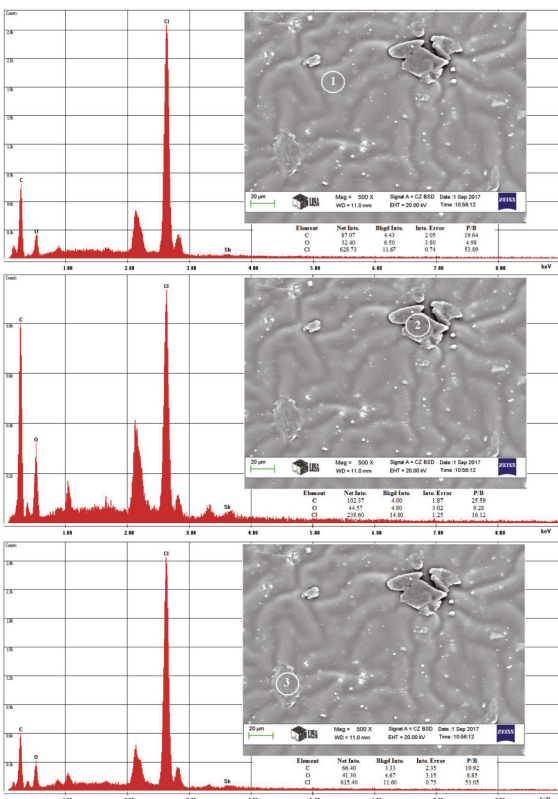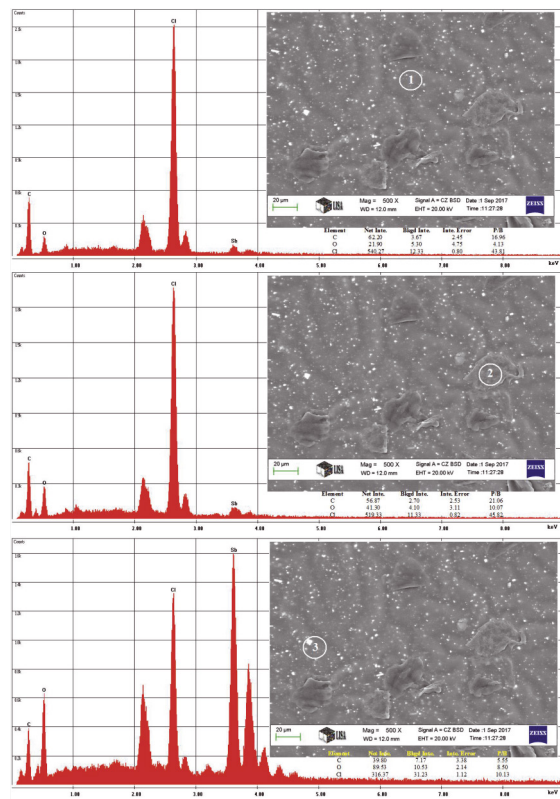7. ábra SEM - energia diszperzív röntgen mikroanalízis a HAZ az elégetett lágyított PVC-ben. Sb_2O_3 tartalom 5%

4. Conclusions

The PVC combustion is not confined to the flame exposed layer but extends beyond the burning layer. Experiments have shown a decrease in chlorine content in the non burning heat affected zone. Without Sb_2O_3 ease of ignition of heat affected zone was observed due to structural changes. The heat affected zone has a low inclination of ignition and is immediately flame retardant if the compound contains Sb_2O_3 because the $SbCl_3$ is already present in this layer.

5. Acknowledgements

References

[1] Al-Mosawi, A. I. (2016): Flammability of composites, Chapter 14, in Njuguna, J. (ed.) Lightweight composite structures in transport: Design, manufacturing, analysis and performance. UK: , pp.361-369. ISBN: 978-1-78242-325-6 (print), ISBN: 978-1-78242-343-0 (online). DOI: https://doi.org/10.1016/B978-1-78242-325-6.00014-1

[2] Al-Mosawi, A. I. (2003): Study using of antimony trioxide material as a flame retardant material, M.Sc. thesis , Babylon University, Iraq .

[3] Al-Maamori, M. H. – Al-Mosawi, A. I. (2014): Increasing resistance of polymeric composite materials to elevated temperatures by coating with antimony tetroxide material, Central Organization for Standardization and Quality Control (COSQC), No.3743, International Classification (C08C19/30), Iraqi Classification (4).

[4] Horrocks, A. R. – Price, D. (eds.) (2008): Advances in Fire Retardant Materials, 1st edn., *CRC Press*, October 7. ISBN: 9781420079616.

[5] Morgan, J. H. (ed.), (2016): SFPE Handbook of Fire Protection Engineering, 5th edition, *Springer*, ISBN 978-1-4939-2564-3, 978-1-4939-2565-0 (eBook).

[6] Al-Mosawi, A. I. (2012): Flame Retardancy of Polymers, *LAP LAMBERT Academic Publishing*, ISBN: 25531 -659 -3-978.

[7] Morley, J. C. – Grossman, R. F. (2008): Flame Retardants and Smoke Suppressants, in Grossman, R.F., (Ed.), Handbook of Vinyl Formulating, 2nd edition, *John Wiley and Sons*, New York, N.Y. , pp. 403-414, ISBN 978-0-471-71046-2, https://doi.org/10.1002/9780470253595.ch16

[8] Le Bras, M. G. – Camino, Bourbigot, S. – Delobel, R. (eds.) (1998): Fire Retardancy of Polymers - The Use of Intumescence, *The Royal Society of Chemistry*.

[9] Technical information (2013): Flame retardant mechanism of antimony trioxide, *Nihon Seiko Co., Ltd.*, Japan.

[10] Coaker, A.W. (2003): Fire and Flame Retardants for PVC, Journal of Vinyl &Additive Technology, vol. 9, no. 3, pp. 108-115. https://doi.org/10.1002/vnl.10072

[11] Al-Mosawi, A.I . – Ahmed, J. K. – Hussain, H. A. (2012): Evaluation flame retardancy of epoxy composite by using design of experiments, in OPTIROB 2012, Applied Mechanics and Materials , vol.186, pp 156-160. https://doi.org/10.4028/www.scientific.net/AMM.186.156

[12] Rodolfo, Jr. A. – Innocentini-Mei, L. H. (2017): Smoke suppression of PVC and copper (II), molybdenum and zinc oxides mixtures: TG/MS and TG/FTIR studies, in Proc.PVC 2017, p. 25-27.

[13] The Vinyl Institute, (1996): Fire and polyvinyl chloride - Vinyl in Design, A Division of The Society of the Plastics Industry, Inc.65 Madison Avenue, Morristown, New Jersey.

[14] Al-Mosawi, A. I. – Marossy, K. (2017): Performance Evaluation of Mixing Mechanism and its Effects on Thermal Behaviour of Plasticised PVC, *International Journal of Engineering and Technology (IJET)*, Vol.9, No.6, pp.4389-4396. https://doi.org/10.21817/ijet/2017/v9i6/170906130

[15] Marcelo H. (2017): Fire properties of polyvinyl chloride, The Vinyl Institute, Washington, DC, USA.

[16] Babrauskas, V. – Harris, R. H. – Gann, R. G. – Levin, B. C. – Lee, B. T. – Peacock, R. D. – Paabo, M. – Twilley, W. – Yoklavich, M. F. – Clark, H. M. (1988): Fire Hazard Comparison of Fire Retarded and Non-Fire-Retarded Products, *NBS Special Publication* 749.

[17] Sheng, G. Z. – Si-yuan, M. – WANG, H. (2007): Inorganic Flame Retardant and Smoke Suppressant in Flexible PVC, *Journal of Hengshui University*, Vol.9, No.1, pp. 93-96.

Eltérő őrölhetőségű anyagok együttőrlésének alapvizsgálata univerzális Hardgrove malomban

GREGUS Éva ▪ Miskolci Egyetem ▪ ejtgrege@uni-miskolc.hu
RÁCZ Ádám ▪ Miskolci Egyetem ▪ ejtracz@uni-miskolc.hu
CSŐKE Barnabás ▪ Miskolci Egyetem ▪ ejtcsoba@uni-miskolc.hu

Intergrinding of materials with different grindability in Universal Hardgrove mill
The most energy and price consuming process in a mineral processing technology is grinding. In this study materials with different grindability were prepared and used for separate and intergrinding experiments. Quartz and limestone were used for the two components intergrinding, where the quartz is hard to grind and non-adhesive, but the limestone is easy to grind and adhesive. The grinding experiments were carried out in a Universal Hardgrove Mill. The ground material was examined in laser particle size distribution analyser and optical microscope to determine the particle size distribution and investigate the particle shape as well. During the grinding experiments grinding work was measured based on torque measurement. In case of intergrinding the material composition in different size fractions were determined by loss on ignition measurement. The Bond work index of the materials were calculated from the torque measurement results. Based on the measurement results the different grinding behaviour of the quartz and limestone can be seen. The limestone was fractured easily at the beginning of grinding, while at longer grinding times sticking and agglomeration of the particles occurred, while the efficiency of the grinding was significantly decreased. Contrary, quartz was fractured slightly in the grinding chamber, only attrition of the particles surface occurs and not body breakage. This can be traced back to the spherical shape of the quartz particles. Based on the results of the intergrinding it can be conclude that the increasing limestone content in the feed resulted in ground material with lower particle size and higher specific surface at a constant specific grinding work. The material composition of the ground materials in different size fractions showed that the limestone was enriched in the fine (<20 µm) fraction at the intergrinding. The quartz particles participate in the grinding like a grinding media. From the intergrinding of different size fractions of one material it can be conclude that the grinding of quartz resulted in high amount of fine, less than 1 µm product. So, in this case as well mainly the attrition of the quartz particles was carried out.
Keywords: Two components intergrinding, Universal Hardgrove mill
Kulcsszavak: Kétkomponensű együttőrlés, Universal Hardgrove malom

GREGUS Éva
2017-ben szerzett Bsc diplomát a Miskolci Egyetem Műszaki Földtudományi Karán, műszaki földtudományi alapszakon, nyersanyagelőkészítési specializáción. Jelenleg tanszéki mérnökként dolgozik az Miskolci Egyetem, Nyersanyagelőkészítési és Környezeti Eljárástechnikai Intézetében a „Fenntartható Nyersanyag-gazdálkodási Tematikus Hálózat – RING 2017" című, EFOP-3.6.2-16-2017- 00010 jelű projekt keretében.

RÁCZ Ádám
2008-ban végzett a Miskolci Egyetem, Műszaki Földtudományi Karán, előkészítéstechnikai mérnök szakon. Doktori (PhD) fokozatát 2014-ben szerezte őrlés tématerületén. Jelenleg a Miskolci Egyetem, Nyersanyagelőkészítési és Környezeti Eljárástechnikai Intézetének adjunktusa. Fő kutatási és oktatási területe a mechanikai eljárástechnika és az aprítás, őrlés.

CSŐKE Barnabás
A Miskolci Egyetem, Műszaki Földtudományi Karának Professzor Emeritusza. Okleveles bányamérnökként végzett 1969-ben a Miskolci Egyetem, Bányamérnöki Karán. Műszaki tudomány kandidátusa címet 1976-ban, PhD fokozatát 1986-ban szerezte. 1997-ben Habilitációs fokozatot szerzett. 1998-2016 között egyetemi tanár a Miskolci Egyetemen. Fő kutatási és oktatási területei a mechanikai eljárástechnika, aprítás, őrlés, hulladékelőkészítés.

1. Bevezetés

Az egyik legnagyobb energiaigényű nyersanyag-előkészítési folyamat az aprítás, őrlés [1,2] és ennek köszönhetően jelentős költséghányadot képvisel egy ásványelőkészítési technológia üzemeltetésében. Annak érdekében, hogy az energiafelhasználást minimalizálni tudjuk az üzemi és gépi pataméterek optimálása az őrlendő anyagok tulajdonságainak ismeretében kiemelt fontosságú feladat. Az eltérő őrölhetőségű anyagok együttőrlésére számos alkalmazást találunk az iparban, kiemelt példája a cementiparban a klinker egyéb hidraulikus kötőanyagokkal és töltőanyagokkal keverékként való őrlése. A folyamatok megértéséhez ki kell emelni, hogy az együttőrlés során a különböző őrölhetőségű szemcsék hatással vannak egymásra, a nagyobb méretű és nehezebben őrölhető anyag szemcséi kvázi őrlőtestként működhetnek vagy a finomabb anyag bevonatot képezhet a nagyméretű és nehezebben őrölhető szemcsék felületén. *Csőke és társai* [3] különböző őrölhetőségű anyagok Bond és Hardrove malomban való együttőrlésével foglalkoztak, a különböző módon meghatározott Bond-indexek eltérését vizsgálták. Méréseiket összekapcsolták az alkotórészek tö-

megarányának meghatározásával az őrleményben, az őrléseket nem az őrölhetőségi koefficiens állandósult állapotáig hajtották végre, hanem az alkotórészek összetételbeli kémiai egyensúlyáig folytatták le. *Ipek* [4] szerint a lágyabb komponenst tartalmazó keverékek Bond munkaindexei nagyobbak, mint az egyedi alkotók munkaindexeinek súlyozott átlaga a keverékekben. *Öner* [5] a Bond mérést klinker és kohósalak keverékén végezte el. Megmutatta, hogy a keverékek Bond őrölhetősége alacsonyabb, mint az összetevők őrlésének súlyozott átlaga az összes salak hozzáadása esetén. Együttőrlésnél az alacsonyabb őrölhetőségű salak a durvább frakcióban halmozódik fel, míg a klinker a nagyobb őrölhetőség miatt a finomabb frakcióban dúsul. *Abouzeid és Fuerstenau* [6] a nagy nyomású őrlőhengereket (HPGR) vizsgálták. Rávilágítottak, hogy a nagy keménységű ásványi részecskék energiatranszferként működnek a hengerek réseiben és fokozzák a puhább ásványi részecskék őrlését a kevert feladásban. *Tavares* [7] szerint a durvább szemcsék által a HPGR-ben tapasztalt nagyobb gyengülés csökkenti az energia-megtakarítást és a termék további őrlésének finomabb méretét. *Ellerbrock és munkatársainak* [8] eredményei alapján a cementkomponensek részecskeméret-eloszlása függ az őrlő-

rendszer típusától és működési módjától, valamint a cement-komponensek őrölhetőségétől. *Faitli és munkatársai* [9] üzemi vizsgálatokat hajtottak végre az őrlési energiaigény optimalizálása érdekében egy vertikális görgős malomban, melyhez léces szélosztályozó kapcsolódik. Kifejlesztésre került egy finomítási és három szétválasztási szakasz a minőségi termék előállítása céljából. Több mintavételi pont és modellezés segítségével állapították meg az optimalizáláshoz szükséges anyagáramokat és a légszeparátor fordulatszámát. Az üzemi adatokból Bond munkaindex került számításra. A fentiekkel összefüggésben a kutatómunka célja a kétkomponensű rendszerek együttőrlésének vizsgálata univerzális Hardgrove malomban és az őrlés során lejátszódó szemcse kölcsönhatásoknak a vizsgálata.

2. Anyagok és eljárások

A méréseket és vizsgálatokat a Nyersanyagelőkészítési és Környezeti Eljárástechnikai Intézet laboratóriumaiban és eszközein végeztük el. A kétkomponensű őrlési kísérletekhez kvarcot és mészkövet használtunk. Első lépésként előállítottuk a méréshez megfelelő kiindulási alapanyagokat. Laboratóriumi szitákat használva 106-250 µm és 32-106 µm közötti frakciókat hoztunk létre nedves szitálással, majd szárítószekrényben 105 °C-on kiszárítottuk a frakciókat. Az őrlési kísérletekhez univerzális Hardgrove malmot alkalmaztunk. Univerzalitása abban található, hogy nem csak az őrlési körülmények, hanem a hőmérséklete is változtatható 20–300 °C között, illetve képes az őrléshez szükséges munka direkt mérésére nyomatékmérés segítségével. A berendezés fejlesztés egyik célja az volt, hogy az üzemi viszonyokat jobban megközelítő, magasabb hőmérsékleteken is el lehessen végezni az őrölhetőségi vizsgálatokat. Ezért a malmot (az őrlőtégelyt) a fűtését szolgáló tégelykemencével vették körül [2, 11]. Az őrlések során a szabványos Hardgrove őrlés körülményeit alkalmaztuk (8 db őrlőgolyó, F= 290 N, fordulatszám 20 1/perc). Minden őrlési kísérlet során az univerzális Hardgrove malomra V_H=58 cm³-nek megfelelő tömegű anyag került feladásra [10].
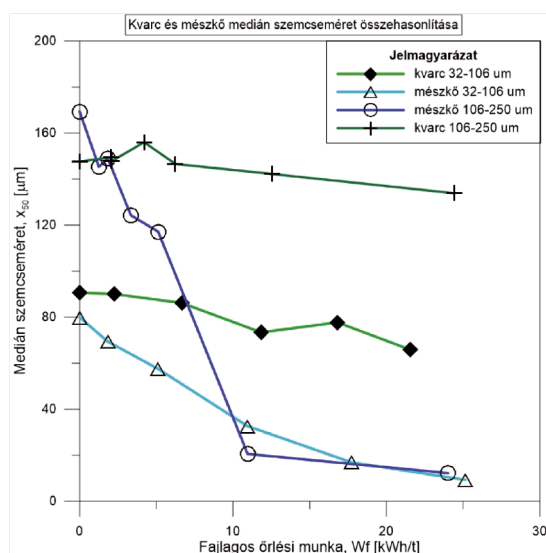
A fajlagos őrlési munka (W_f) értékek a nyomatékmérésen alapuló mérési eredményekből ($W_{f,mért}$) kerültek meghatározásra minden őrlési kísérlet során. A kiindulási anyagok és az őrlemények empirikus szemcseméret eloszlását és a számított fajlagos felületet Horiba LA-950 típusú lézeres szemcseméret elemző segítségével határoztuk meg. A különőrlési vizsgálatok során a kvarcot és mészkövet 3, 5, 10, 15, 30, 60 percig őröltük. A kétkomponensű együttőrlési vizsgálatok során különböző arányú (25-75, 50-50, 75-25) feladásokat állítottunk elő, majd különböző ideig (t=5, 30, 60 min) őröltük őket az univerzális Hardgrove malomban. Ezen felül végeztünk még kísérleteket arra irányulóan is, hogy hogyan viselkedik a mészkő és a kvarc együtt- és különőrlés során, ha saját anyagából kisebb szemcseméretű frakcióval őröljük együtt. Esetünkben mind a kvarc, mind a mészkő 106-250 µm-es frakciójához 32-106 µm-es anyagot kevertünk és együttőrlésnél szintén 5, 30 és 60 percig, különőrlésnél 5, 15, 30, 45 és 60 percig végeztünk rajtuk őrlést 25-75, 50-50, 75-25 arányban keverve a frakciókat. Az együttőrlési kísérletek után az egyes őrleményeken izzítási veszteség mérést is végeztünk. Ehhez az anyagot először frakcionáltuk: 250>x>106µm, x>63µm, x>20µm és 0<x<20µm. Az izzítási veszteség vizsgálatánál analitikai mérleggel mértük a porcelán csónakok tömegét, bemértünk 1 g anyagot, majd szobahőmérsékletű kemencébe helyeztük a mintákat. A kemence 1,5 óra alatt érte el a 950 °C hőmérsékletet, majd további 1 órát volt még benn az anyag. Kihűlés után mértük a tömegeket és meghatároztuk az izzítási veszteségeket.

3. Mérési eredmények

3.1 Különőrlési eredmények

A vizsgálatok során elvégeztük a mészkő és kvarc szemcsék külön őrlését, majd eltérő összetételek mellet vizsgáltuk az őrlemények diszperzitás jellemzőinek változását és az anyagok őrlés közben egymásra gyakorolt hatását. Az *1. ábrán* a kvarc és mészkő két különböző frakciójának különőrlési eredménye ta-

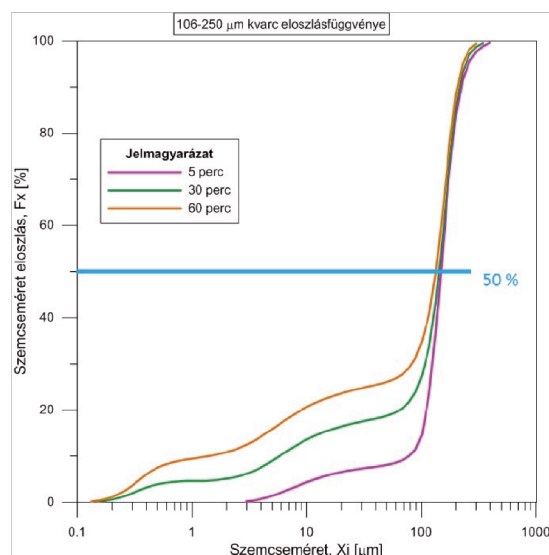*1. ábra* Mészkő és kvarc mediánjának változása a fajlagos őrlési munka függvényében különőrlés esetén
Fig. 1 Median particle size of limestone and quartz as a function of the specific grinding work in case of separate grinding
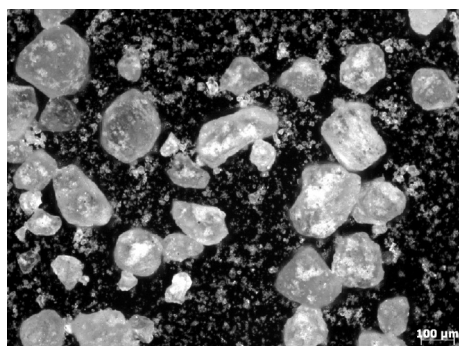

2. ábra Kvarc szemcseméretének eloszlásfüggvénye különőrlés esetén
Fig. 2 Cummulative undersize of quartz in case of separate grinding
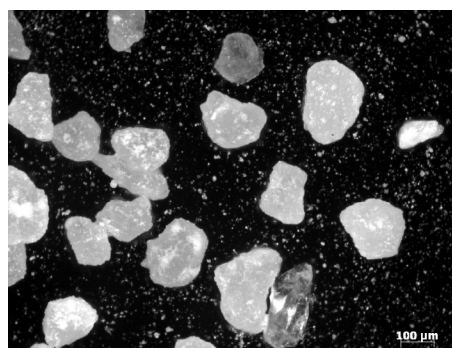
a)

a)

b)

b)

3. ábra Kvarc szemcsék mikroszkópi felvételei (a, kiindulási; b, 60perc)
Fig. 3 Microscopic picture of quartz particles, a-feed, b -60 min grinding

4. ábra Mészkő szemcsék mikroszkópi felvételei (a, kiindulási; b, 60perc)
Fig. 4 Microscopic picture of limestone particles, a-feed, b -60 min grinding

lálható, ahol a medián változása látható a fajlagos őrlési munka függvényében. A kvarc kiindulási medián szemcsemérete 106-250 μm-es frakciónál 147,6 μm-ről 133,9 μm-re csökkent 25 kWh/t fajlagos őrlési munka befektetése után. Mészkő esetén az anyag jelentős szemcseméret csökkenésen esett át, a kiindulási medián szemcseméret 169,4 μm-ről 12,23 μm-re csökkent 24 kWh/t fajlagos őrlési munka hatására. A kisebb, 32-106 μm-es kvarc frakció csak kismértékű szemcseméret változás következett be, 91 μm-ről 66 μm-re mérséklődik a szemcsemért 21 kWh/t fajlagos őrlési munka következtében, a mészkőnél a nagyobb frakcióhoz hasonlóan jelentős a változás, 80 μm-ről 9,3 μm-re csökkent a medián szemcseméret 25 kWh/t fajlagos őrlési munka után. A kvarc esetén a medián szemcseméret változása és a fajlagos őrlési munka között lineáris összefüggést figyelhetünk meg. Ezzel ellentétben a mészkő 106-250 μm-es frakció esetében 11 kWh/t munka és 13 μm eléréséig lineárisan csökken a szemcseméret, míg ezután 24 kW/t fajlagos őrlési munka esetén sem csökken jelentősen tovább a szemcseméret. A finomabb mészkő frakció esetében a szemcseméret csökkenése lineáris a fajlagos őrlési munkával. A kvarc-szemcsék a befektetett őrlési munka és a közölt – a Hardgrove malomban kialakuló – igénybevételek hatására nem, vagy csak alig törtek, a medián szemcseméret kismértékű csökkenése figyelhető meg a befektetett fajlagos őrlési munka függvényében. Megvizsgálva a kvarc 106-250 μm-es frakciójának szemcseméret-eloszlás változását az őrlési idő függvényében (*2. ábra*), azt láthatjuk, hogy habár a medián szemcseméret alig változott, a finomabb (<50 μm) szemcseméret tartományban az anyag jelentősen finomodott, a <50 μm-es rész tömeghányada jelentősen megnőtt 7 %-ról 28 %-ra. Az 1 μm alatti szemcsék mennyisége a kvarcőrleményben szintén jelentősen növekedett ~ 1 %-ról
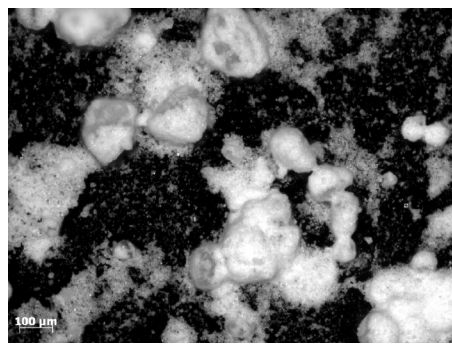
10-13%-ra (*2. ábra*). Mindeközben a fajlagos felület is erőteljesen növekedett, kvarc esetén 326 cm²/g-ról 8054 cm²/g-ra a 106-250 μm-es frakciónál és 1085 cm²/g-ról 8971 cm²/g-ra a 32-106 μm-es frakció esetében. Mészkő vizsgálatánál a 106-250 μm-es frakciónál 907 cm²/g-ról 2673 cm²/g-ra, a 32-106 μm-es frakciónál pedig 1242 cm²/g-ról 11297 cm²/g-ra növekedett. Ennek magyarázatára azt mondhatjuk, hogy a fellépő dörzsölő igénybevétel csak koptatta a szemcsék felületét, miközben a kvarcszemcsék nagy része megőrzi az eredeti méretét, tehát teljes szemcsetörés nem következett be az őrlés során. A *3. ábrán* a kvarc kiindulási és 60 perces őrlés utáni állapotának Zeiss mikroszkópos felvétele látható. A szemcsék lekerekítettek, kevés törési felület, éles rész észlelhető rajtuk. A felületi koptatás hatására kialakult kerekded szemcsealak a jellemző. A 60 perces őrlés után a szemcséken lényeges változásként csak az tapasztalható, hogy még lekerekedettebb formát nyertek a kezdetihez képest. A mészkőőrlemény mikroszkópi felvételén látszik, hogy az őrlemény szemcséi inkább szögletesebbnek mutatkoznak, mint a kvarcőrlemény szemcséi. A *4. ábrán* a mészkő kiindulási és 60 perces őrleményének mikroszkópos felvételei láthatóak. A szemcsék alapvetően szabálytalan alakúak, sok törési felülettel. A 60 perces őrlés követően a nagyobb méretű szemcsék felülete simább lett, az alakjuk lekerekítetté, gömbszerűbbé vált. A kvarc szemcsék nehezebb őrölhetőségét vizsgálva *Mucsi* [2] munkássága alapján, arra következtetünk, hogy a szferikus alakkal rendelkező kvarc, hasonlóan az általa vizsgált klinkerhez kisebb őrlési ellenállást fejt ki, mint a kubikusabb szemcsealakkal rendelkező mészkő, ezért nem szenved megfelelő mértékben törést a szemcse. Valószínűleg a kvarc szemcsék behúzása az őrlőtest által csak részben történik meg. Az anyagok őrlés során eltérő viselkedésének bemutatá-

5. ábra   Mészkő őrlése – jelentős feltapadás
Fig. 5   Limestone grinding – significant adhesion

6. ábra   Kvarc őrlése – nincs feltapadás
Fig. 6   Quartz grinding – no adhesion

sára a betapadást is vizsgáltuk (*5. ábra*), mely alapján megállapítható hogy a kvarc esetén nem tapasztalható feltapadás az őrlőtestekre és a malom falazatára, míg, a mészkőnél viszont ez több grammnyi mennyiségű anyagréteg is felrakódott, elsősorban az őrlőtestek felületére. Az őrlőtestek felületén keletkező bevonat rontja az őrlési hatékonyságot, mely magyarázza a medián szemcseméret és a fajlagos őrlési munka közötti nem linearitást a 106-250 µm-es frakció őrlése során. A tiszta mészkő őrlésénél keletkező finom töretrész az őrlési idő hosszabbodásával az őrlőtesten bevonatot képez (*5. és 6. ábra*).

3.2 Kvarc és mészkő együttőrlési eredményei

Együttőrlés során a 25, 50, és 75 térfogatszázalékos keverékek szemcseméret változásait vizsgáltuk. A mészkőtartalom növekedésével a feladási anyagban egyre finomabb őrleményt kapunk adott fajlagos őrlési munka befektetése mellett. A *7. ábrán* látható, hogy a magasabb mészkőtartalmú keverékek (50 és 75%) medián szemcsemérete alacsonyabb adott fajlagos őrlési munka mellett, mint a 100%-os mészkő őrlése esetén. Az utol-

só mérési pontban (60 perces őrlés) a medián szemcsemérete az 50 és 75%-os mészkőtartalmú keveréknek kisebb 5,75 µm és 3,12 µm, mint a tiszta mészkőé, 12,23 µm. A 25% mészkövet tartalmazó őrlési görbe a tiszta kvarcéval közel megegyező, de a kis mészkőtartalomnak köszönhetően simább lefutású, kismértékű szemcseméret csökkenéssel (114,9 µm) (*7. ábra*).

A *8. ábrán* a 60 perces őrlést követően vizsgáltuk az anyagok szemcseméretsűrűség függvényét 106-250 µm-es frakció esetén. Az értékek bimodális görbéket írnak le. A 100%-os mészkő tartalomnál a módusz a durvább szemcseméret nagyság felé tolódik el. A 75%-os mészkőtartalom esetén a gyakoriság értéke felcserélődik az 50 és a 100%-os görbékhez képest, itt a módusz értéke a finomabb szemcseméret frakcióban van. A csúcsértékeknél a szemcseméret alakulása: 50% mészkőtartalom esetén 152,45 µm; 75% mészkőtartalom esetén 2,27 µm; 100% mészkőtartalom esetén 152,45 µm. A *9. ábrán* a 106-250 µm-es frakciójú kvarc-mészkő együttőrlés medián szemcseméretei kerültek feltüntetésre a kvarc tartalom függvényében 10 és 20 kWh/t fajlagos munkaszükséglet mellett. A feladott anyag kvarc tartalmának növelésével a medián
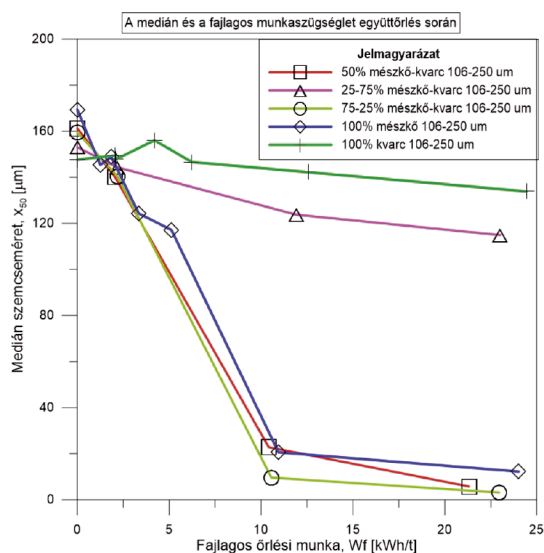
7. ábra   A medián változása a fajlagos őrlési munkaszükséglet függvényében mészkő-kvarc együttőrlése során
Fig. 7   The median particle size as a function of the specific grinding work in case if limestone-quartz intergrinding
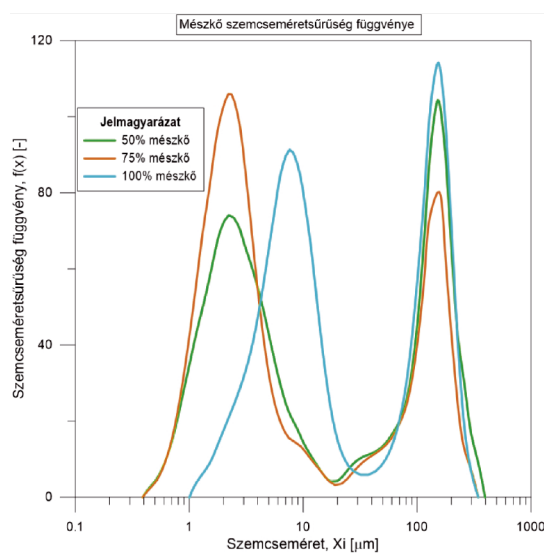
8. ábra   106-250 µm-es frakció szemcseméret-sűrűségfüggvénye 60 perces mészkő-kvarc együttőrlésnél
Fig. 8   Particle size density function of 106-250 µm fraction at 60 min limestone-quartz intergrinding
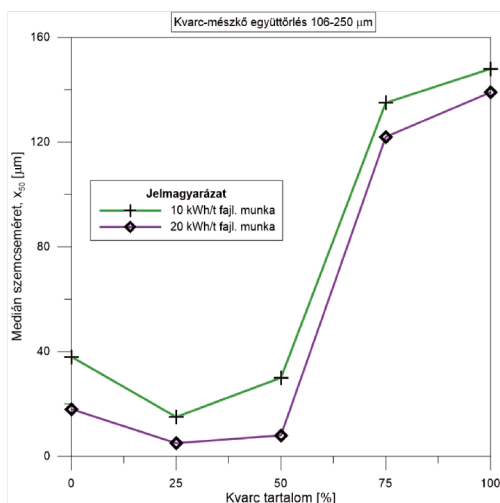
9. ábra   Medián szemcseméret változása a kvarc tartalom függvényében
Fig. 9   Median particle size as a function of the quartz content
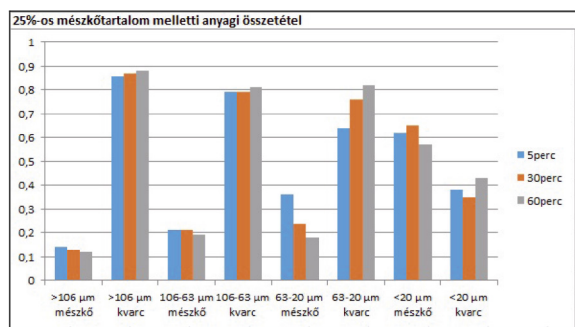
a,
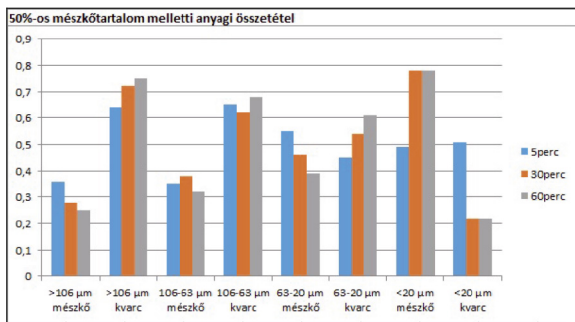
b,
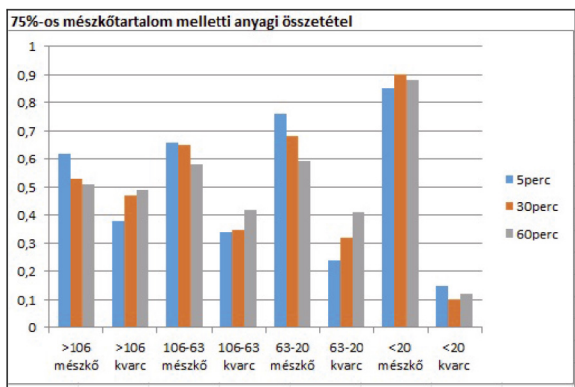
c

10. ábra   Az őrlemény anyagi összetétele kvarc-mészkő együttőrlés esetén
Fig. 10   Material composition of the ground material in case of quartz-limestone intergriding

szemcseméret a durvább szemcsenagyságok felé tolódik el. Az együttőrlés 25%-os kvarc tartalom mellett a legideálisabb, ekkor a legkisebbek az 50%-os szemcsemérethez tartozó értékek. 10 és 20 kWh/t fajlagos őrlési munka befektetésnél is az 50%-os kvarc adagolás alacsonyabb medián szemcseméretet eredményezett az őrleményben, mint a tiszta mészkő esetén. Ezt azzal magyarázhatjuk, hogy a kvarc jelenléte az őrleményben csökkentette a finom szemcsék összetapadásának mértékét, illetve a kvarc szemcsék kvázi őrlőtestként részt vettek az őrlési folyamatban. A kvarc-mészkő együttőrlési kísérleteket követően a különböző őrlési időknél kapott őrleményeket szemcseméret frakciókra bontottuk, majd anyagi összetételt határoztunk meg az egyes frakciókon, hogy lássuk a mészkő és kvarc frakciónkénti eloszlását. Az összetétel eredményeket a *10. ábra* mutatja. A vizsgálatból megállapítható, hogy a mészkő a <20 µm-es tartományban feldúsul, míg a kvarc inkább a durva szemcseméret tartományban dúsul fel (*10. ábra*). A 25%-os mészkőtartalom esetén a legdurvább >106 µm-es frakcióban a mészkő tömeghányada jelentősen lecsökken, 14%-ra már 5 perces őrlést követően, majd tovább csökken az őrlési idővel, ebben a frakcióban párhuzamosan ezzel a kvarc tömeghányada 86%-ra nő, majd folyamatosan nő az őrlési idővel. A 63-106 µm-es frakcióban ugyanez a tendencia figyelhető meg, habár ebben a frakcióban a mészkőtartalom közelebb áll a kiindulási 25%-hoz, értéke 20% körül változik az őrlési idővel. A 20-63 µm-es frakcióban a kiindulási állapothoz képest 5 perces őrlési időnél több a mészkő 35%, majd folyamatosan csökken az őrlési idővel 18%-ra. A <20 µm-es részben a mészkőtartalom jelentősen eltér az eredeti 25%-os értékről. 5 perces őrlésnél 49% a mészkőtartalom, majd az őrlési idővel tovább nő egészen 78%-ig. Az 50%-os mészkőtartalom esetén a > 106 µm-es tartományban a mészkő tömeghányada hasonlóan alakul a 25%-os őrléséhez, értéke 25%-ra csökken 60 perc őrlést követően. A kvarc tömeghányada itt is nő 75%-ra. A 63-106 µm-es frakcióban a mészkő- és kvarctartalom lényegében nem változik, a 20-63 µm-es tartományban pedig a kiindulási értékhez áll közel, ~50% a mészkőtartalom. A < 20 µm-es frakcióban a mészkő a 30 perces őrlés után feldúsul. Értéke nagymértékben eltér a kiindulásítól, közel 80% lesz. A 75%-os mészkőtartalomnál a > 106 µm-es tartományban a mészkő tömeghányada 62%-ról 51%-ra csökken az őrléseket követően, míg a kvarc értékei 49%-ra nőnek. A 63-106 µm-es frakcióban a mérés eredményeiben nagy ingadozás nem jelentkezik, a mészkőtartalom 60% körül alakul. A 20-63 µm-es szemcseméret tartomány esetében a 75%-os mészkőtartalom jelentősen lecsökken, 60 perc elteltével csak 59% lesz, a kvarc értéke 41%-ra nő a kiindulási 25%-ról. A legkisebb szemcseméret frakcióban itt is a mészkő feldúsulása figyelhető meg. Legnagyobb értékét a 30 perces őrlés után veszi fel, itt a dúsulás mértéke 90%, majd kis mértékben csökken.

3.3 Különböző szemcseméretű együttőrlések eredményei

A további vizsgálatok során mindkét anyagnál a saját, de eltérő szemcseméretű (106-250 µm és 32-106 µm) minták keveréke került feladásra. A kvarc eltérő szemcseméret frakciójának őrléséből származó medián értékeket a fajlagos őrlési munka függvényében a *11. ábrán* láthatjuk. Az őrlemény medián szemcsemérete lineáris csökkenést mutat a befektetett munka függvényében. Az eltérő frakciók együttőrlésénél a medián
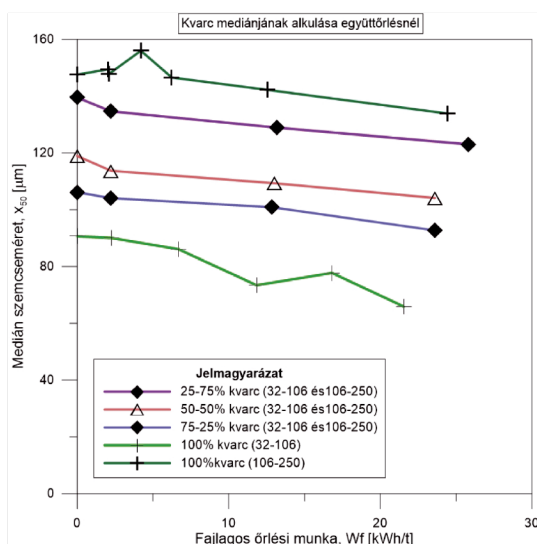
11. ábra   Az őrlemény mediánjának alakulása különböző szemcseméretű kvarc frakciók együttőrlésnél
Fig. 11   Median particle size at the intergrinding of quatz with different size fractions
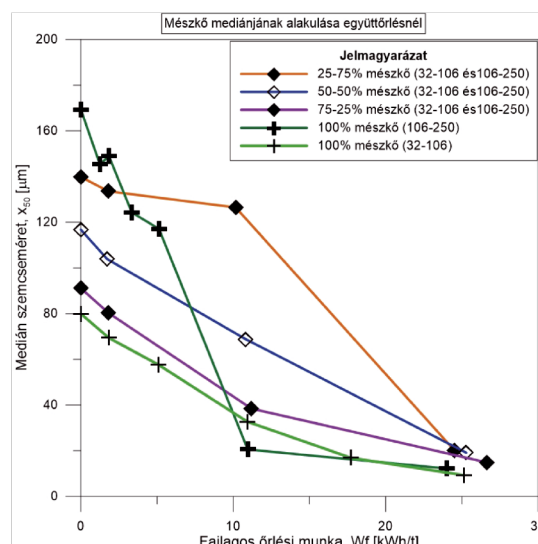
12. ábra   Medián változása különböző méretű mészkő frakciók együttőrlésekor
Fig. 12   Median particle size at the intergrinding of limestone with different size fractions

szemcseméret közel azonos mértékben csökken a fajlagos őrlési munka befektetésének függvényében. Megállapítható, hogy minél inkább a 32-106 μm-es frakciójú anyag mennyisége növekszik a keverékben, annál jobban közelítik a görbék ennek a frakciónak a tiszta őrlési eredményeit. A mészkő különböző frakcióinak együttőrlése eredményét a *12. ábrán* mutatjuk be. A medián vizsgálata során látható, hogy minden anyagi összetételnél jelentősen csökken a medián szemcseméret a fajlagos őrlési munka függvényében (*12. ábra*). Mindhárom keverék esetében a 25 kWh/t fajlagos őrlési munka befektetés hatására 20 μm közeli őrlemény medián értéket kapunk. A *13. ábrán* az eltérő szemcsefrakciók együttőrlésének medián szemcseméret értékei láthatók 10 és 20 kWh/t befektetett fajlagos munka mellett a kisebb, 32-106 μm-es frakció függvényében vizsgálva. Kvarc együttőrlése során, minél több a feladás finomrész tartalma, annál kisebb lesz a medián szemcseméret is. Mészkőnél azt tapasztaltuk, hogy 0 és 100% finomrész tartalomnál is ugyan az a medián szemcseméret a vizsgált fajlagos munkáknál.

4. Összefoglalás

A kutatómunka során különböző őrölhetőségű anyagok együttőrlési vizsgálatát végeztük el univerzális Hardgrove malomban. A kétkomponensű együttőrléshez kvarcot és mészkövet alkalmaztunk, a kvarc nehezen őrölhető, de tapadásra nem hajlamos, míg a mészkő könnyen őrölhető és aggregációra, tapadásra hajlamos anyag. A különőrlési mérési eredményeink bemutatták a mészkő és a kvarc eltérő viselkedését az őrlés során. A mészkő az őrlési folyamat kezdetén könnyen aprózódott, majd az őrlés előrehaladtával jelentős betapadás volt megfigyelhető az őrlőtérben, miközben az őrlés hatékonysága jelentősen csökkent. Ezzel szemben a kvarc csak kis mértékben aprózódott az őrlőtérben, jellemzően csak felületi koptatás történt a teljes szemcsetörés helyett, mely visszavezethető a kvarc szemcsék gömbszerű szemalakjára. Az együttőrlési mérési eredményeink alapján megállapítható, hogy a mészkőtartalom növelésével a feladásban egyre finomabb őrleményt
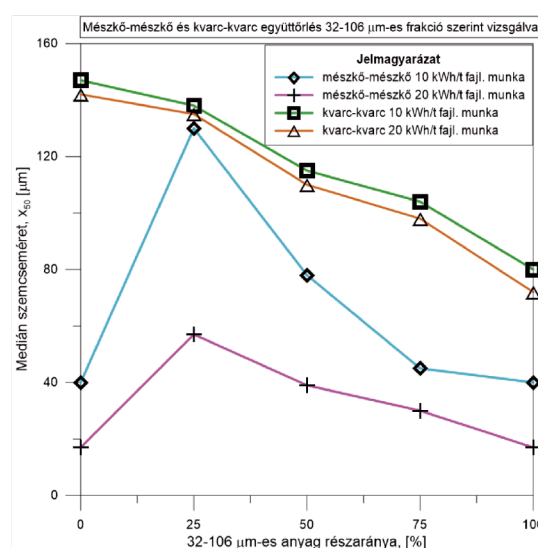
13. ábra   Medián szemcseméret változása a 32-106 μm-es frakció részaránya szerint kvarc és mészkő különböző méretű frakcióinak együttőrlésekor
Fig. 13   Median particle size as a function of the mass percent of 32-106 μm fraction at the intergrinding of quatz and limestone with different size fractions

kaptunk adott fajlagos őrlési energia befektetés esetén. Az őrlemények anyagi összetételének frakciónkénti meghatározásából megállapítható, hogy a finomabb mészkő feldúsul a kvarccal történő együttőrlés során a finom, <20 μm-es tartományban. Méréseink alapján megállapítható, hogy a keményebb anyag az együttőrlés során elősegíti az őrlést, egyrészről az adhéziós erők lekötésével, más részről az őrlési folyamatban kvázi őrlőtestként való részvételként.

5. Köszönetnyilvánítás

Hivatkozások

[1] Csőke B. (2005): Előkészítéstechnika: Aprítás és osztályozás, *Miskolci Egyetem*, Eljárástechnika Tanszék

[2] Mucsi G. (2009): Vizsgálati eljárások fejlesztése finom szemcseméretű anyagok őrölhetőségének, valamint különleges körülmények mellett történő őrlés energiaszükségletének meghatározása, Doktori értekezés, *Miskolci Egyetem*

[3] Csőke B. – Rácz Á. – Mucsi G. (2013): Determination of the Bond work index of binary mixtures by different methods, *International Journal of Mineral Processing*, 123 78–86, https://doi.org/10.1016/j.minpro.2013.05.004

[4] Ipek, H. – Ucbas, Y. – Hosten, C. (2005 a): The bond work index of mixtures of ceramic raw materials. *Miner. Eng.* 18, 981 983 (1), https://doi.org/10.1016/j.mineng.2004.12.014

[5] Öner, M., (2000): A study of intergrinding and separate grinding of blast furnace slag cement. *Cem. Concr. Res.* 30, 473-480, https://doi.org/10.1016/S0008-8846(00)00197-6

[6] Abouzeid, A.-Z. M. – Fuerstenau, D. W. (2009): Grinding of mineral mixtures in high-pressure grinding rolls. *Int. J. Miner. Process.* 93, 59, 65, https://doi.org/10.1016/j.minpro.2009.05.008Get rights a

[7] Tavares, L. M. (2005): Particle weakening in high-pressure roll grinding. *Miner. Eng.* 18 (7), 651-657, https://doi.org/10.1016/j.mineng.2004.10.012

[8] Ellerbrock, H. G. – Sprung, S. – Kuhlmann, K. (1990): Particle size distribution and properties of cement, Part III: in fl uence of the grinding process. *Zement-Kalk-Gips* 3/1990, Edition B. 13 19,

[9] Faitli József – Czél Péter (2014): Matrix modell simulation of a Vertical Roller Mill with High-Efficiency Slat Classifier, *Chem. Eng. Technol. 37*, No. 5, 1–9, https://doi.org/10.1002/ceat.201300665

[10] Mag G. A. (2015)Térfogati alapú körfolyamatos őrölhetőségi vizsgálati módszerellenőrzése, *Miskolci Egyetem*, Szakdolgozat

[11] Mucsi G. (2008) Fast test method for the determination of the grindability of fine materials, *Chemical Engineering Research and Design*, 86:(4) pp. 395-400, https://doi.org/10.1016/j.cherd.2007.10.015

About CEES

CEES is the organisation representing the European Silicate Industry. It brings together Western European Producers of Soluble Silicates. CEES is a Sector Group of Cefic.

CEES members manufacture more than 700,000 tonnes (1998 figures) of soluble silicates (calculated as SiO_2) representing more than 90% of total West European production. More than half this production is used as a feedstock raw material for further chemical manufacture, mostly silicas and aluminosilicates. Overall, the silicate industry makes a valuable contribution to the Western European economy.

CEES members operate modern, fuel-efficient plants maintaining the highest standards of health and safety to protect both the workforce and the environment. All CEES members full support and implement the Europe-wide Cefic Responsible Care initiative.

www.cees-silicates.org
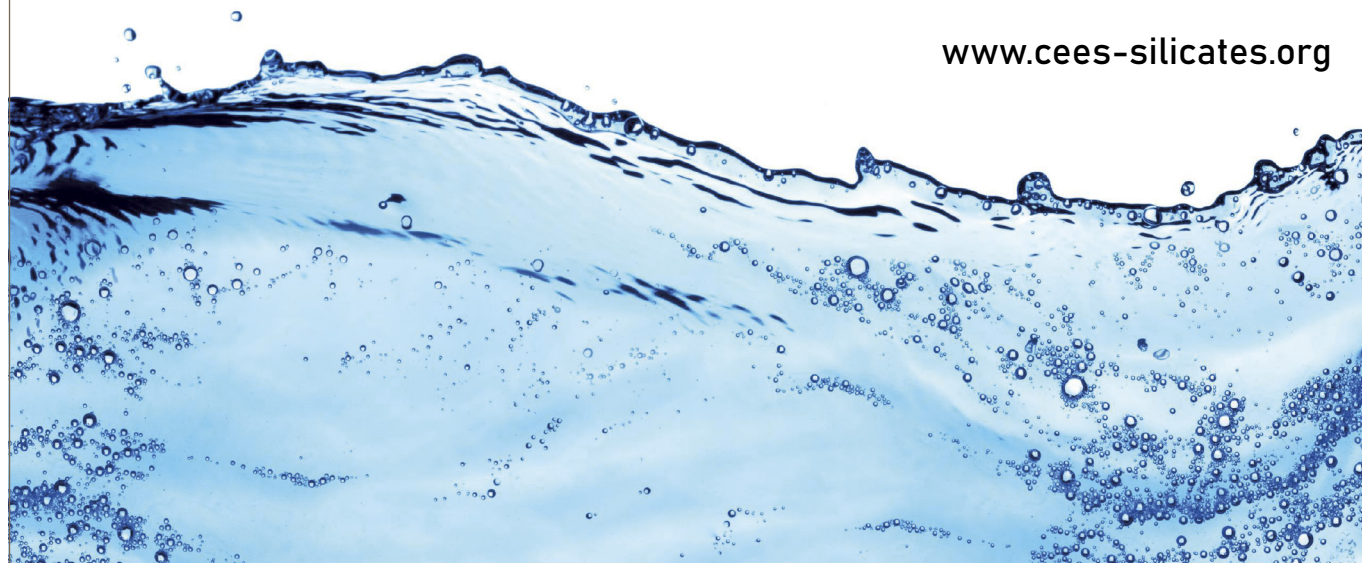
CompIC

COMPOSITES IN CONSTRUCTION CONFERENCE
10th - 11th Apr 2019 • Amsterdam Science Park, Amsterdam, Netherlands

Composites in Construction

Reinforcing the Future of the Modern Built Environment
CompIC 2019 will continue to expand and explore the success stories, advantages and obstacles of using composites in construction applications.

Join the debate and discover common interests in developing fibre reinforced polymer composites as the material of choice for an increasing number of construction and infrastructure projects.

The next European CompIC conference and exhibition will take place at the Science Park in Amsterdam, 10-11 April 2019.

This conference attracts an audience of professional end-users, architects, asset owners, composite manufacturers, material suppliers, consultancies, designers, researchers and academics.

The call for papers is now open and you can register now to secure your place at CompIC 2019 and hear about the latest developments in fibre reinforced composite construction materials.

www.compositesin.construction

Understanding the mechanism of decomposition reactions of neat and superplasticized ordinary Portland cement pastes using thermal analysis

ELSHAFIE A. M. GAD ▪ Egyptian Petroleum Research Institute ▪ eamgad@gmail.com

AMR OSMAN HABIB ▪ Chemistry Dept. Faculty of Engineering, Ain Shams University, Cairo ▪ amrhabib2004@yahoo.com

MAHMOUD M. MOUSA ▪ Faculty of Science, Benha University, Egypt ▪ mousa_chem@yahoo.com

Prof. Dr. Elshafie A. GAD
Professor of Petrochemicals. My interests are surfactants applications, QSPR, Computational chemistry and recently Solid state Kinetics.

Dr. Amr Osman HABIB
received his M.Sc and Ph.D from Ain Shams University, Cairo, Egypt. He is currently a lecturer at Faculty of Engineering, Ain Shams University. He is a member of Technology of Building Materials and Pore Structure of Solids Unit, (R & D Unit), Faculty of Science, Ain Shams University, and member of The Engineering Consultants Centre, Faculty of Engineering, Ain Shams University.

Prof. Dr. Emeritus, Mahmoud M. MOUSA,
Faculty of Science, Benha University, his interests are treatment of industrial solid wastes, renal function Studies, Iminodiacetic Acid Analog, Nanomaterials application and solid state kinetics.

Abstract

The effect of polycarboxylate superplasticizer on thermal stability and the kinetic thermal decomposition of OPC without and with 1.0 and 1.5% wt% plasticizer has been studied at temperature range of 30-1000 °C. The study was done by means of thermogravimetry (TG) technique under non-isothermal condition at a heating rate of 10 K/min. The results showed that the decomposition occurs for the superplasticized and neat OPC paste in three steps. The neat OPC was found to decompose at higher temperatures than those for the superplasticized paste. The kinetic parameters for each one of the decomposition steps were calculated through four calculation methods and the kinetic mechanisms were determined from the thermal data analysis using 35 solid state reaction models. The results showed that the mechanisms of decomposition steps depend on the percentage of the superplasticizer added to the paste. The thermodynamic parameters $\Delta S^{\#}$, $\Delta H^{\#}$ and $\Delta G^{\#}$ were also computed and discussed.
Keywords: Hydration kinetics, Ordinary Portland cement OPC, Thermogravimetric analysis TGA

1. Introduction

Calcium silicate hydrates (CSH) and calcium hydroxide (CH) which are the main hydration phases accounted for the properties of Portland cement paste. The dehydration of Portland cement paste causes a deterioration effect on the concrete strength. Thermal analysis tools can be used to identify each of the product compositions and their amounts due to thermal effects on cement composites. Several investigators studied thermal analysis to recognize the products due to hydration of different cement composites [1,2,3]. Zelic et al. [4] investigated thermal decomposition kinetics of the calcium hydroxide-Portlandite formed into hydrated ordinary Portland cement (OPC) paste with use of non-isothermal thermogravimetric data. Sha et al. [5] reported that the three major endothermic peaks in the DSC curves are due to loss of water from calcium silicate hydrate, dehydroxyaltion of calcium hydroxide, and decarbonation of calcium carbonate contribute respectively. Pane et al. [6] investigated hydration of OPC pastes containing three types of mineral additive; fly ash, ground-granulated slag, and silica fume using DTA/TGA and isothermal calorimetry It was shown that the chemically bound water obtained using DTA/TGA was proportional to heat of hydration and could be used as a measure of hydration. Agarwal et al. [7] studied the hydration behavior of different cements at different time intervals in the presence of superplasticizers using DTA technique. It was observed that OPC has shown retardation either blended with naphthalene-based superplasticizers or with blended polymer-based superplasticizer. However, Portland Slag Cement has been found to be compatible with all the superplasticizers. Ye et al. [8] reported on the

properties of Self-compacting when it is exposed to elevated temperatures. Fire test has shown differences between high performance concrete and traditional concrete at elevated temperature. These differences are largely depending on the microstructural properties of concrete matrix. Kong et al. [9] studied the effect of elevated temperature on geopolymer paste, mortar and concrete made using fly ash as a precursor. It was found that strength loss in geopolymer concrete at elevated temperatures is attributed to the thermal mismatch between the geopolymer matrix and the aggregates. Heikal et al. [10] studied the effect of substitution of nano-silica on the behavior of composite cement pastes including OPC and blast-furnace slag exposed to elevated temperature up to 1000°C. DTA and TGA were carried out on cement pastes partially replaced with Neem seed husk ash [11]. The results showed that the calcium hydroxide contents increases with increase in Neem seed husk ash replacements. Klimesch and Ray [12] presented a method for consistent DTA/TGA evaluation using computer software for data analyses. DTA/TGA was used to study the effect of ground quartz addition to cement. Alarcon-Ruiz et al. [13] used thermal analysis techniques to study the effect of temperature in the mineralogical composition of cement hydration products. Such techniques can be used to determine fire conditions and the consequent deterioration expected in the cement paste. Bhatty and Reid [14] produces high-strength Type 1 cement. The product from raw taconite and copper-nickel tailings of Minnesota is the subjected to hydration studies by using thermal methods such as TGA and DTA. Hydration is measured in terms of hydration product formation and the amount of bound water and free calcium hydroxide incorporated in them.

Oxide	SiO$_2$	Al$_2$O$_3$	Fe$_2$O$_3$	CaO	MgO	SO$_3$	Na-Oxide	K- Oxide	Lime Saturation Factor	Undissolved solids	Loss on Ignition
%	19.82	4.99	3.92	62.66	0.82	2.53	0.47	0.09	0.95	0.97	3.92

Table 1. Chemical analysis of ordinary Portland cement
1. táblázat   Tiszta portlandcement kémiai összetétele

Reactions that occur with an increase of temperature in cement paste and concrete can be summarized as: evaporable water and a part of the bound water escapes at 30–102°C [4]. The decomposition of gypsum [15] and ettringite [16] takes place at 110–170°C, The decomposition of the C-S-H and carboaluminate hydrates undergoes at 180–300°C [17]. Dehydroxylation of the portlandite [18] occurs at 450–550°C. Decarbonation of calcium carbonate happens at 700–900°C [13].

However, the dehydration kinetics of Portland cement paste is too complex and can not be described by a single Arrhenius equation. In the present work, we studied the thermal dehydration and decomposition kinetics of OPC hardened pastes containing polycarboxylate admixtures using TGA at a heating rate of 10 K/min for two samples containing admixtures besides, control sample. Four calculation procedures based on TG curves as well as 35 mechanism functions were applied on the thermal data.

2. Materials and experimental technique

2.1 Cement

A freshly produced sample of a commercial ordinary Portland cement supplied from Suez Cement Company with the chemical composition listed in *Table 1*, was used in this study.

The specific surface area as determined by the Blaine air-permeability method was found to be 3400 cm2/gm. The potential phase composition as estimated using Bogue's calculation [19] was found to be C3S, 58.04; β-C2S, 13.11; C3A, 6.59 and C4AF, 11.91, respectively.

2.2 Preparation of OPC pastes

The percentages of admixtures (1.0 & 1.5 wt %) were dissolved in water of mixing. Various cement pastes were prepared by mixing OPC with water using standard water of consistency for each paste. The control cement pastes and the superplasticized samples with 1.0 and 1.5 wt % were hydrated for 28 days.

The standard water of consistency and percentage of water reduction were listed in *Table 2*.

Paste	W/C ratio	Water reduction %
Neat OPC	0.245	0 %
OPC+1%1%	0.1712	30%
OPC+1.5 %	0.16	34.69 %

Table 2. The standard water of consistency and percentage of water reduction for the control and superplasticized cement pastes
2. táblázat   Szabványos víztartalom és vízcsökkenés mértéke a kontroll és folyósító adalékszerrel kezelt minták esetén

2.3 Thermal analysis

The thermal decomposition of the different hardened cement pastes was studied by thermal gravimetric analysis (TGA) technique using Simultaneous TGA/DSC MODEL SDTQ 600 Thermal Analyzer (USA). Some grains were extracted from the inner core of the hardened cement pastes. These grains were crushed and ground until a grain size of 80 μm was obtained. The temperature of the furnace was programmed to rise as a constant heating rate of 10 °C/min up to 1000 °C

3. Background on non-isothermal decomposition kinetics

Kinetic process calculations result in three parameters; i. e., Ea is the activation energy, A is the pre-exponential factor, f(α) represents the mathematical form of the mechanism to be assumed for the process, and α is the conversion degree. The rate determining mechanism model may take various forms based nucleation and nucleus growth, phase boundary reaction, diffusion and chemical reaction [20].

The reaction rate equation for non-isothermal decomposition kinetics [20] can be written as follows:

$$\frac{d\alpha}{dt} = k(T)f(\alpha) \tag{1}$$

Where k is the rate constant and the conversion factor α is defined as:

$$\alpha = \frac{m_i - m_t}{m_i - m_\infty} \tag{2}$$

Where m_i is the initial mass of the sample, m_t is the mass of the sample at time t, and m_∞ is the residual mass of the sample at the end of the reaction.

Integration of Eq. (1) gives the integral rate law:

$$g(\alpha) = kt \tag{3}$$

The rate constant k is generally given by the Arrhenius equation:

$$k = A \, exp(\frac{-E_a}{RT}) \tag{4}$$

Where E$_a$ is the activation energy, R is the gas constant, and T is the absolute temperature. The combination of Eqs. (1) and (4) gives the following relationship:

$$\frac{d\alpha}{dt} = A \, exp(\frac{-E_a}{RT})f(\alpha) \tag{5}$$

For a dynamic TG process, introducing the heating rate, β = dT/dt, into Eq. (5), gives Eq. (6):

$$\frac{d\alpha}{dt} = \left(\frac{A}{\beta}\right) exp(\frac{-E_a}{RT})f(\alpha) \tag{6}$$

No.	Symbol	Name of the function	$g(\alpha)$	$f(\alpha)$	Rate-determining mechanism
			1. Chemical process or mechanism non-invoking equations		
1	$F_{1/3}$	One-third order	$1 - (1 - \alpha)^{2/3}$	$(3/2)(1 - \alpha)^{1/3}$	Chemical reaction
2	$F_{3/4}$	Three-quarters order	$1 - (1 - \alpha)^{1/4}$	$4(1 - \alpha)^{3/4}$	Chemical reaction
3	$F_{3/2}$	One and a half order	$(1 - \alpha)^{-1/2} - 1$	$2(1 - \alpha)^{3/2}$	Chemical reaction
4	F_2	Second order	$(1 - \alpha)^{-1} - 1$	$(1 - \alpha)^2$	Chemical reaction
5	F_3	Third order	$(1 - \alpha)^{-2} - 1$	$(1/2)(1 - \alpha)^3$	Chemical reaction
			2. Acceleratory rate equations		
6	$P_{3/2}$	Mampel power law	$\alpha^{3/2}$	$(2/3)\alpha^{-1/2}$	Nucleation
7	$P_{1/2}$	Mampel power law	$\alpha^{1/2}$	$2\alpha^{1/2}$	Nucleation
8	$P_{1/3}$	Mampel power law	$\alpha^{1/3}$	$3\alpha^{2/3}$	Nucleation
9	$P_{1/4}$	Mampel power law	$\alpha^{1/4}$	$4\alpha^{3/4}$	Nucleation
10	E_1	Exponensial law	$\mathrm{Ln}\,\alpha$	A	Nucleation
			3. Sigmoidal rate equations or random nucleation and subsequent growth		
11	A_1, F_1	Avrami–Erofeev equation	$-\ln(1 - \alpha)$	$(1 - \alpha)$	Assumed random nucleation and its subsequent growth, n = 1
12	$A_{3/2}$	Avrami–Erofeev equation	$[-\ln(1 - \alpha)]^{2/3}$	$(3/2)(1 - \alpha)[-\ln(1 - \alpha)]^{1/3}$	Assumed random nucleation and its subsequent growth, n = 1.5
13	A_2	Avrami–Erofeev equation	$[-\ln(1 - \alpha)]^{1/2}$	$2(1 - \alpha)[-\ln(1 - \alpha)]^{1/2}$	Assumed random nucleation and its subsequent growth, n = 2
14	A_3	Avrami–Erofeev equation	$[-\ln(1 - \alpha)]^{1/3}$	$3(1 - \alpha)[-\ln(1 - \alpha)]^{2/3}$	Assumed random nucleation and its subsequent growth, n = 2.5
15	A_4	Avrami–Erofeev equation	$[-\ln(1 - \alpha)]^{1/4}$	$4(1 - \alpha)[-\ln(1 - \alpha)]^{3/4}$	Assumed random nucleation and its subsequent growth, n = 3
16	A_u	Prout–Tomkins equation	$\ln[(\alpha/(1 - \alpha)]$	$\alpha(1 - \alpha)$	Assumed random nucleation and its subsequent growth, n = 4 Branching nuclei
			4. Deceleratory rate equations		
			4.1. Phase boundary reaction		
17	R_1, F_0, P_1	Power law	α	$(1 - \alpha)^0$	Contracting disk
18	$R_2, F_{1/2}$	Power law	$1 - (1 - \alpha)^{1/2}$	$2(1 - \alpha)^{1/2}$	Contracting cylinder (cylindrical symmetry)
19	$R_3, F_{2/3}$	Power law	$1 - (1 - \alpha)^{1/3}$	$3(1 - \alpha)^{2/3}$	Contracting sphere (spherical symmetry)
			4.2. Based on the diffusion mechanism		
20	D_1	Parabola low	α^2	$\frac{1}{2}\alpha$	One-dimensional diffusion
21	D_2	Valensi equation	$\alpha + (1 - \alpha)\ln((1 - \alpha)$	$[-\ln(1 - \alpha)]^{-1}$	Two-dimension diffusion
22	D_3	Jander equation	$[1 - (1 - \alpha)^{1/3}]^2$	$(3/2)(1 - \alpha)^{2/3}[1 - (1 - \alpha)^{1/3}]^{-1}$	Three-dimensional diffusion, spherical symmetry
23	D_4	Ginstling–Brounstein equation	$1 - 2\alpha/3 - (1 - \alpha)^{2/3}$	$(3/2)[(1 - \alpha)^{-1/3} - 1]^{-1}$	Three-dimensional diffusion, cylindrical symmetry
24	D_5	Zhuravlev, Lesokin, Tempelman equation	$[(1 - \alpha)^{-1/3} - 1]^2$	$(3/2)(1 - \alpha)^{4/3}[(1 - \alpha)^{-1/3} - 1]^{-1}$	Three-dimensional diffusion
25	D_6	anti-Jander equation	$[(1 + \alpha)^{1/3} - 1]^2$	$(3/2)(1 + \alpha)^{2/3}[(1 + \alpha)^{1/3} - 1]^{-1}$	Three-dimensional diffusion
26	D_7	anti-Ginstling-Brounstein equation	$1 + 2\alpha/3 - (1 + \alpha)^{2/3}$	$(3/2)[(1 + \alpha)^{-1/3} - 1]^{-1}$	Three-dimensional diffusion
27	D_8	anti-Zhuravlev, Lesokin, Tempelman equation	$[(1 + \alpha)^{-1/3} - 1]^2$	$(3/2)(1 + \alpha)^{4/3}[(1 + \alpha)^{-1/3} - 1]^{-1}$	Three-dimensional diffusion
			5. Another kinetics equations with unjustified mechanism		
28	G_1		$1 - (1 - \alpha)^2$	$\frac{1}{2}(1 - \alpha)$	
29	G_2		$1 - (1 - \alpha)^3$	$1/3(1 - \alpha)^2$	
30	G_3		$1 - (1 - \alpha)^4$	$\frac{1}{4}(1 - \alpha)^3$	
31	G_4		$[-\ln(1 - \alpha)]^2$	$(1/2)(1 - \alpha)[-\ln(1 - \alpha)]^{-1}$	
32	G_5		$[-\ln(1 - \alpha)]^3$	$(1/3)(1 - \alpha)[-\ln(1 - \alpha)]^{-2}$	
33	G_6		$[-\ln(1 - \alpha)]^4$	$(1/4)(1 - \alpha)[-\ln(1 - \alpha)]^{-3}$	
34	G_7		$[1 - (1 - \alpha)^{1/2}]^{1/2}$	$4\{(1 - \alpha)[1 - (1 - \alpha)^{1/2}]^{1/2}$	
35	G_8		$[1 - (1 - \alpha)^{1/3}]^{1/2}$	$6(1 - \alpha)^{2/3}[1 - (1 - \alpha)^{1/3}]^{1/2}$	

Table 3. Algebraic expressions of functions g(α) and f(α) and its corresponding mechanism [20]
3. táblázat Az g(α) és f(α) függvények algebrai alakjai és a meghatározó mechanizmusok [20]

	Decomposition step		Kinetic models			
			Eq 7	Eq 8	Eq 9	Eq 10
OPC	1st step	Mechanism	F3/2	F3/2	F3/2	F2
		Max R²	**0.9969**	**0.9969**	**0.9969**	**0.9941**
		Ea	**99.764**	**99.764**	**99.910**	**115.2940**
		A	3.171E+13	2.764E+14	3.51913E+13	1.42983E+16
	2nd step	Mechanism	G6	P1/4	G6	G6
		Max R²	**0.9968**	**0.9993**	**0.9968**	**0.9973**
		Ea	**1313.022**	**50.837**	**1317.998**	**1339.6461**
		A	2.838E+90	2.599E+03	3.05568E+93	7.87165E+94
	3rd step	Mechanism	Au	D7	G6	G6
		Max R²	**0.9948**	**0.9955**	**0.9912**	**0.9933**
		Ea	**614.035**	**275.823**	**802.540**	**805.8707**
		A	1.107E+32	4.103E+13	2.02021E+45	2.40603E+45
OPC+1.0 %	1st step	Mechanism	F3/2	D5	D5	D5
		Max R²	**0.9988**	**0.9993**	**0.9993**	**0.9994**
		Ea	**46.839**	**95.010**	**95.158**	**93.8318**
		A	5.750E+05	8.550E+12	1.08953E+12	6.51732E+11
	2nd step	Mechanism	G8	D7	D1	D1
		Max R²	0.9906	0.9956	0.9799	0.9688
		Ea	-7.889	85.079	91.518	93.8317
		A	-4.440E-03	4.412E+04	189154.1585	281841.940
	3rd step	Mechanism	Au	P1/4	D5	G6
		Max R²	**0.9941**	**0.9977**	**0.9937**	**0.9920**
		Ea	**825.910**	**47.965**	**719.201**	**1337.9727**
		A	8.463E+42	1.531E+02	6.73532E+36	9.34991E+72
OPC+1.5%	1st step	Mechanism	G8	F2	F2	F2
		Max R²	**0.9969**	**0.9965**	**0.9965**	**0.9970**
		Ea	**-3.388**	**60.676**	**60.863**	**61.7420**
		A	-8.774E-	9.514E+08	122772431.9	163422155.
	2nd step	Mechanism	G8	D7	G6	G6
		Max R²	**0.9845**	**0.9945**	**0.9620**	**0.9598**
		Ea	**-8.314**	**86.000**	**268.665**	**270.7971**
		A	-4.269E-	3.074E+04	2.96196E+20	3.21247E+20
	3rd step	Mechanism	G6	P1/4	D5	D5
		Max R²	**0.9976**	**0.9988**	**0.9982**	**0.9984**
		Ea	**1653.171**	**62.673**	**898.848**	**886.3492**
		A	9.769E+85	1.044E+03	6.97492E+45	1.42405E+45

Table 4. *Kinetic parameters, activation energy (Ea) and the pre-exponential (A) calculated from Coats et al., Eq. (7), Wanjun et al., Eq. (8), Madhysudanan et al., Eq. (9) and Tang et al., Eq. (10), according to maximum correlation coefficients out of 35 models of mechanism of decomposition of different cement pastes*

4. táblázat *Kinetikai paraméterek, aktiválási energia (Ea) és hatványkitevő (A), Coats et al., Eq. (7), Wanjun et al., Eq. (8), Madhysudanan et al., Eq. (9) and Tang et al., Eq. (10) alapján számítva, 35 különböző cementpép lebomlási modell legnagyobb korrelációs együtthatója alapján*

Decomposition step	OPC	OPC+1.0%	OPC+1.5%
Dehydration	$F_{3/2}$ – Chemical reaction	D5 – Three-dimensional diffusion	F2 – Second order reaction
Dehydroxylation	G6 – Unjustified mechanism	D1 – One dimensional diffusion	G6 – Unjustified mechanism
Decarbonation	G6 – Unjustified mechanism	P ¼ – Nucleation	P ¼ – Nucleation

Table 5. *Summary of the rate determining mechanism of the thermal decomposition steps of the neat cement pastes and the superplasticized cement pastes with 1.0 and 1.5%*

5. táblázat *Tiszta portlandcementpép, valamint 1,0 és 1,5% folyósító adalékszert tartalmazó cementpépek hőbomlásának meghatározó mechanizmusai*

4. Results and discussion

Thermograms (TGA and DTG) curves of OPC containing polycarboxylate admixtures (dose = 1.0 or 1.5%) and the control sample are shown in *Figs. 1* and *2*. The curves show three weight loss zones. The first drop in weight ranging from 100 to 200 °C, is accounted for the dehydration of Ca-silicate hydrates. The second weight loss is displayed at 450 to 500 °C which is attributed to dehydroxyaltion of portlandite. The third loss of weight shown at 700 to 750 °C, is due to decarbonation of calcium carbonate. The thermal analyses data are summarized in *Table 3*. It shows that the modified OPC Samples decompose at higher temperatures than that found for untreated OPC. This refers to that the addition of polycarboxylate admixture increases the thermal stability of OPC.
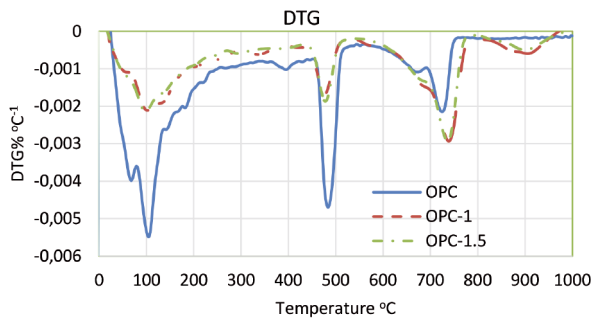

Fig. 1. DTG curves of the thermal decomposition of OPC containing polycarboxylate, heating rate = 10 Kmin⁻¹

1. ábra Polikarboxilát tartalmú portlandcementpépek hőbomlása DTG görbékkel szemléltetve (felfűtési sebesség = 10 Kmin⁻¹)
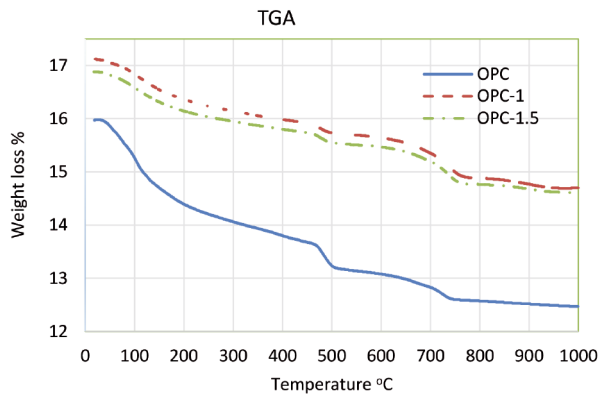

Fig. 2. TGA curves of the thermal decomposition of OPC containing polycarboxylate, heating rate = 10 Kmin⁻¹

2. ábra Polikarboxilát tartalmú portlandcementpépek hőbomlása TGA görbékkel szemléltetve (felfűtési sebesség = 10 Kmin⁻¹)

The kinetic parameters for the three stages of the thermal decomposition of the investigated samples were calculated using fraction conversion 0.1< α <0.8 obtained from a single thermos-analytical curve (heating rate 10 K/min). In this study, four calculation methods: Coats and Redfern [21], Eq. (7), Madhysudanan-Krishnan-Ninan [22], Eq. (8), Wanjun et al. [22], Eq. (9) and Tang et al. [23], Eq. (10) as as well as 35 mechanism models g(α) were used to get the kinetic data:

$$\ln\left(\frac{g(\alpha)}{T^2}\right) = \ln\left[\frac{AR}{\beta E_a}\left(1 - \frac{2RT}{E_a}\right)\right] - \frac{E_a}{RT} \cong \ln\left(\frac{AR}{\beta E_a}\right) - \frac{E_a}{RT} \quad (7)$$

$$\ln\left(\frac{g(\alpha)}{T^2}\right) = \ln\left[\frac{AR}{\beta(1.00198882E + 1.87391198RT_p)}\right] - \frac{E_a}{RT} \quad (8)$$

$$\ln\left[\frac{g(\alpha)}{T^{1.894661}}\right] = \left[\ln\frac{AE_a}{\beta R} + 3.635041 - 1.89466\ lnE_a\right] - \frac{1.00145033E_a}{RT} \quad (9)$$

$$\ln\left[\frac{g(\alpha)}{T^{1.921503}}\right] = \left[\frac{\ln AE_a}{\beta R} + 3.772050 - 1.921503 lnE_a\right] - \frac{0.120394E_a}{T} \quad (10)$$

Plotting the left-hand sides of Eqs. (7-10), which involves g(α) versus 1/T, gives E_a and A from the slope and intercept, respectively. The model that gives the higher correlation coefficient of the linear regression R^2 for Eqs. (7) – (10) fit is chosen as the selected kinetic model. A mathematical program based on Excel 2016 was designed by the authors to calculate values of activation energy Ea and the pre-exponential as shown in *Table 4*.

The best mechanisms for each decomposition step, the kinetic results of the applied equations show kinetic models and parameters close to each other in the most cases as shown in *Table 4*. From which the best kinetic models according to the highest correlation coefficients and the kinetic parameters are given in *Table 5*. It can be seen that the mechanism of step depends on the percentage of the superplasticizer.

The pre-exponential factor A is calculated from the intercept of the plots of Eqs. (7-10), and from the theory of the activated complex (transition state) of Eyring [24,25], the following general equation may be written:

$$A = \frac{ek_BT_p}{h}exp\left(\frac{\Delta S^{\neq}}{R}\right) \quad (17)$$

Where: e = 2.7183 is the Neper number; k_B – Boltzmann constant; h – Plank constant, and T_p is the peak temperature of DTG curve.

According to the values of activation energy E and pre-exponential factor A for the different stages of decomposition, The calculated values of ΔS≠, ΔH≠ and ΔG≠ are calculated using Eqs. (18 – 20) at T = T_p (T_p is the DTG peak temperature at the corresponding stage), because this temperature characterizes the highest rate of the decomposition process. Therefore, the change of the activated entropy can be calculated according to the formula:

$$\Delta S^{\neq} = R\ln\frac{Ah}{ek_BT_p} \quad (18)$$

Since

$$\Delta H^{\neq} = E - RT_p \quad (19)$$

The changes in the activated enthalpy $\Delta H^{\neq}$ and the Gibbs free energy $\Delta G^{\neq}$ for the activated complex formation from the reactant are calculated using the well-known thermos-dynamical equation:

$$\Delta G^{\neq} = \Delta H^{\neq} - T_p\Delta S^{\neq} \quad (20)$$

The thermodynamic results obtained are given in *Table 6*. From which it can be seen that the $\Delta S^{\neq}$ value for the first decomposition stage of the hardened cement past is positive. It means that the activated complexes are less order in the arrangement, higher entropy. However, first decomposition stages of plasticized samples with 1.0 and 1.5% show negative values of $\Delta S^{\neq}$ it means that the corresponding activated

complex more arrangement lower entropy. While for the 2nd and 3rd decomposition stage, the corresponding activated complexes have negative values of $\Delta S^{\neq}$ referring to higher degree of arrangement, i.e lower entropy than the initial state.

Decomposition step		OPC	OPC+1.0%	OPC+1.5%	Units
Dehydration	$\Delta S^{\#}$	4.24	-28.92	-97.85	J/mol.K
	$\Delta H^{\#}$	96.80	90.72	58.63	kJ/mol
	$\Delta G^{\#}$	95.22	101.51	95.13	Kj/mol
Dehydroxylation	$\Delta S^{\#}$	-195.22	-171.67	-174.68	J/(mol.K)
	$\Delta H^{\#}$	44.81	79.049	79.97	kJ/mol
	$\Delta G^{\#}$	185.95	203.17	206.26	Kj/mol
Decarbonation	$\Delta S^{\#}$	-2.45	-221.23	-205.27	J/(mol.K)
	$\Delta H^{\#}$	267.71	39.85	54.56	kJ/mol
	$\Delta G^{\#}$	270.10	255.11	254.28	Kj/mol

Table 6.   *Thermodynamic parameters for different stages of thermal decomposition of hardened neat cement paste and plasticized cement paste*
6. táblázat   *Megszilárdult tiszta cementpép és folyósító adalékszert tartalmazó cementpép hőbomlásának termodinamikai paraméterei a lebomlás különböző fázisaiban*

5. Conclusions

The addition of polycarboxylate superplasticizer into OPC with 1 and 1.5 wt% increased its thermal stability without any change in the thermal decomposition products. Whereas, the kinetic study showed that the mechanism for each decomposition step depends on the percentage of plasticizer found in the OPC sample.

6. Compliance with Ethical Standards

The authors declare that they have no conflict of interest.

References

[1] Sha, W. – Pereira, G.: Differential scanning calorimetry study of ordinary Portland cement paste containing metakaolin and theoretical approach of metakaolin activity. Cem Concr Compos. 2001;23(6):455-461. https://doi.org/10.1016/S0958-9465(00)00090-1

[2] Gruyaert, E. – Robeyst, N. – De Belie, N.: Study of the hydration of Portland cement blended with blast-furnace slag by calorimetry and thermogravimetry. J Therm Anal Calorim. 2010;102(3):941-951. https://doi.org/10.1007/s10973-010-0841-6

[3] Mendes, A. – Sanjayan, J. – Collins, F.: Phase transformations and mechanical strength of OPC/Slag pastes submitted to high temperatures. Mater Struct. 2008;41(2):345-350. https://doi.org/10.1617/s11527-007-9247-8

[4] Zelic, J. – Ugrina, L. – Jozic, D.: Application of Thermal Methods in the Chemistry of Cement: Kinetic of Portlandite from Non-Isothermal Thermogravimetric Data. First Int Profic Test Conf. 2007:420-429.

[5] Sha, W. – O'Neill, E. A. – Guo, Z.: Differential scanning calorimetry study of ordinary Portland cement. Cem Concr Res. 1999;29(9):1487-1489. https://doi.org/10.1016/S0008-8846(99)00128-3

[6] Pane, I. – Hansen, W.: Investigation of blended cement hydration by isothermal calorimetry and thermal analysis. Cem Concr Res. 2005;35(6):1155-1164. https://doi.org/10.1016/j.cemconres.2004.10.027

[7] Agarwal, S. K. – Masood, I. – Malhotra, S. K.: Compatibility of superplasticizers with different cements. Constr Build Mater. 2000;14(5):253-259. https://doi.org/10.1016/S0950-0618(00)00025-8

[8] Ye, G. – Liu, X. – De Schutter, G. – Taerwe, L. – Vandevelde, P.: Phase distribution and microstructural changes of self-compacting cement paste at elevated temperature. Cem Concr Res. 2007;37(6):978-987. https://doi.org/10.1016/j.cemconres.2007.02.011

[9] Kong, D. L.Y. – Sanjayan, J. G.: Effect of elevated temperatures on geopolymer paste, mortar and concrete. Cem Concr Res. 2010;40(2):334-339. https://doi.org/10.1016/j.cemconres.2009.10.017

[10] Heikal, M. – Ali, A. I. – Ismail, M. N. – Ibrahim, S. A. N. S.: Behavior of composite cement pastes containing silica nano-particles at elevated temperature. Constr Build Mater. 2014;70:339-350. https://doi.org/10.1016/j.conbuildmat.2014.07.078

[11] Musa, N. M.: Thermal Analysis of Cement Paste Partially Replaced With Neem Seed Husk Ash. Int J Sci Eng Res. 2014;5(1):1101-1105. http://www.ijser.org.

[12] Klimesch, D. S. – Ray, A.: The use of DTA/TGA to study the effects of ground quartz with different surface areas in autoclaved cement: quartz pastes. Part 1: A method for evaluating DTA/TGA results. Thermochim Acta. 1996;289(1):41-54. https://doi.org/10.1016/S0040-6031(96)03033-X

[13] Alarcon-Ruiz, L. – Platret, G. – Massieu, E. – Ehrlacher, A.: The use of thermal analysis in assessing the effect of temperature on a cement paste. Cem Concr Res. 2005;35(3):609-613. https://doi.org/10.1016/j.cemconres.2004.06.015

[14] Bhatty, J. I. – Reid, K. J.: Use of thermal analysis in the hydration studies of a type 1 portland cement produced from mineral tailings. Thermochim Acta. 1985;91:95-105. https://doi.org/10.1016/0040-6031(85)85205-9

[15] Paulik, F. – Paulik, J. M. A. Thermal decomposition of gypsum. Thermochim Acta. 1992;200:195-204. https://doi.org/10.1016/0040-6031(92)85115-C

[16] Sha, W. – Pereira, G. B.: Differential scanning calorimetry study of ordinary Portland cement paste containing metakaolin and theoretical approach of metakaolin activity. Cem Concr Compos. 2001;23(6):455-461. https://doi.org/10.1016/S0958-9465(00)00090-1

[17] Gard, J. A. – Taylor, H. F. W.: Calcium silicate hydrate (II) ("C-S-H(II)"). Cem Concr Res. 1976;6(5):667-677. https://doi.org/10.1016/0008-8846(76)90031-4

[18] Alarcon-Ruiz, L. – Platret, G. – Massieu, E. – Ehrlacher, A.: The use of thermal analysis in assessing the effect of temperature on a cement paste. Cem Concr Res. 2005;35(3):609-613. https://doi.org/10.1016/j.cemconres.2004.06.015

[19] Skibsted, J. – Jakobsen, H. J. – Hall, C.: Quantification of calcium silicate phases in Portland cements by 29 Si MAS NMR spectroscopy. J Chem Soc …. 1995;91(24):4423-4430.

[20] Vlaev, L. – Nedelchev, N. – Gyurova, K. – Zagorcheva, M.: A comparative study of non-isothermal kinetics of decomposition of calcium oxalate monohydrate. J Anal Appl Pyrolysis. 2008;81(2):253-262. https://doi.org/10.1016/j.jaap.2007.12.003

[21] Abbasi, M. H. – Kahrizsangi, R. E.: Evaluation of reliability of Coats-Redfernnext term method for kinetic analysis of non-isothermal TGA. TransNonfferous Met Soc China. 2008:217-221. https://doi.org/10.1016/S1003-6326(08)60039-4

[22] Georgieva, V. – Vlaev, L. – Gyurova, K.: Non-isothermal degradation kinetics of CaCO3 from different origin. J Chem. 2013;2013. https://doi.org/10.1155/2013/872981

[23] Torkkeli, A.: Droplet microfluidics on a planar surface. VTT Publ. 2003;55(504):3-194. https://doi.org/10.1002/aic

[24] Giese, B. C. H. – Bamford, C. F. H. Tipper (Eds.): Comprehensive Chemical Kinetics, Vol. 16, Liquid-Phase Oxidation, Elsevier, Amsterdam 1980. 264 Seiten, Preis: US $ 87.75. Berichte der Bunsengesellschaft für Phys Chemie. 1981;85(9):721-722. https://doi.org/10.1002/bbpc.19810850935

[25] Dsc CF – Dielectric, B.: Journal of Thermal Analysis and Calorimetry. Vol 91. Kluwer Academic Publishers; 2008. https://doi.org/10.1007/s10973-008-3100-3

The manuscript must contain the followings: title; author's name, workplace, e-mail address; abstract, keywords; main text; **acknowledgement** (optional); **references; figures, photos with notes; tables with notes; short biography** (information on the scientific works of the authors).

The full manuscript should not be more than 6 pages including figures, photos and tables. Settings of the word document are: 3 cm margin up and down, 2,5 cm margin left and right. Paper size: A4. Letter size 10 pt, type: Times New Roman. Lines: simple, justified.

TITLE, AUTHOR
The title of the article should be short and objective.
Under the title the name of the author(s), workplace, e-mail address.
If the text originally was a presentation or poster at a conference, it should be marked.

ABSTRACT, KEYWORDS
The abstract is a short summary of the manuscript, about a half page size. The author should give keywords to the text, which are the most important elements of the article.

MAIN TEXT
Contains: materials and experimental procedure (or something similar), results and discussion (or something similar), conclusions.

REFERENCES
References are marked with numbers, e.g. [6], and a bibliography is made by the reference's order. References should be provided together with the DOI if available.
Examples:
Journals:
[6] Mohamed, K. R. – El-Rashidy, Z. M. – Salama, A. A.: In vitro properties of nano-hydroxyapatite/chitosan biocomposites. *Ceramics International.* 37(8), December 2011, pp. 3265–3271, http://dx.doi.org/10.1016/j.ceramint.2011.05.121
Books:
[6] Mehta, P. K. – Monteiro, P. J. M.: Concrete. Microstructure, properties, and materials. *McGraw-Hill*, 2006, 659 p.

FIGURES, TABLES
All drawings, diagrams and photos are figures. The **text should contain references to all figures and tables**. This shows the place of the figure in the text. Please send all the figures in attached files, and not as a part of the text. **All figures and tables should have a title**.
Authors are asked to submit color figures by submission. Black and white figures are suggested to be avoided, however, acceptable.
The figures should be: tiff, jpg or eps files, 300 dpi at least, photos are 600 dpi at least.

BIOGRAPHY
Max. 500 character size professional biography of the author(s).

CHECKING
The editing board checks the articles and informs the authors about suggested modifications. Since the author is responsible for the content of the article, the author is not liable to accept them.

CONTACT
Please send the manuscript in electronic format to the following e-mail address: femgomze@uni-miskolc.hu and epitoanyag@szte.org.hu or by post: Scientific Society of the Silicate Industry, Budapest, Bécsi út 122–124., H-1034, HUNGARY

We kindly ask the authors to give their e-mail address and phone number on behalf of the quick conciliation.

ESCM

EUROPEAN SOCIETY
FOR COMPOSITE MATERIALS

THE SCIENTIFIC,
ENGIEERING
AND INDUSTRIAL
COMMNITY
INVOLVED WITH
COMPOSITE
MATERIALS

THE SOCIETY

OBJECTIVES OF THE SOCIETY

ESCM is a European, non-governmental, non-profit scientific and engineering organisation with the following objectives:

↘ To encourage the free interchange of information on all those aspects related to composite materials which of are interest to the scientific and engineering community.

↘ To provide a Europe-wide forum for the discussion of such topics, e.g. by organising the ECCM (European Conference on Composite Materials) and more specialised symposia related to composites.

↘ To guide and foster the understanding and utilisation of the science and technology of composite materials.

↘ To promote European co-operation in the study of topics in composite materials science and technology.

↘ To promote liaison with engineering and scientific bodies throughout Europe with similar aims and to serve as a facilitator for communication between such bodies.

↘ To foster an environment for timely and cost-effective research, development and implementation of advanced technology in composites.

↘ To encourage the education of young specialists in the disciplines supporting composite materials science and technology.

↘ To recognise individuals of outstanding achievement in the science, technology, engineering, and application of composite materials.

WWW.ESCM.EU.ORG

In health care, silicones
are the front runner.
And that's a good thing.

Find out why

CES - SILICONES EUROPE

SILICONES & YOU

Silicones have literally thousands of applications that collectively bring safety, comfort and enjoyment to life. They improve the performance and reliability of millions of modern products.

THE SCIENCE

Silicones chemistry is one of the most versatile chemistries on the planet, rendering it full of possibilities and producing a wide range of formulations and uses from aesthetic to technical.

WHO IS CES?

We are a non-profit organisation representing all major producers of silicones in Europe. We provide information on silicones from a health, safety and environmental perspective.

WWW.SILICONES.EU